Cell

Estrogen Prevents Bone Loss via Estrogen Receptor α and Induction of Fas Ligand in Osteoclasts

Takashi Nakamura,[1,2,9] Yuuki Imai,[1,3,9] Takahiro Matsumoto,[1,2] Shingo Sato,[4] Kazusane Takeuchi,[1] Katsuhide Igarashi,[5] Yoshifumi Harada,[6] Yoshiaki Azuma,[6] Andree Krust,[7] Yoko Yamamoto,[1] Hiroshi Nishina,[4] Shu Takeda,[4] Hiroshi Takayanagi,[4] Daniel Metzger,[7] Jun Kanno,[5] Kunio Takaoka,[3] T. John Martin,[8] Pierre Chambon,[7] and Shigeaki Kato[1,2,*]

[1]Institute of Molecular and Cellular Biosciences, University of Tokyo, Yayoi 1-1-1, Bunkyo-ku, Tokyo 113-0032, Japan

[2]Exploratory Research for Advanced Technology, Japan Science and Technology Agency, Honcho 4-1-8, Kawaguchi, Saitama 332-0012, Japan

[3]Department of Orthopaedic Surgery, Osaka City University Graduate School of Medicine, Asahimachi 1-4-3, Abeno-ku, Osaka, 545-8585, Japan

[4]Tokyo Medical and Dental University, Yushima 1-5-45, Bunkyo-ku, Tokyo 113-8510, Japan

[5]Division of Cellular and Molecular Toxicology, National Institute of Health Sciences, 1-18-1 Kamiyoga, Setagaya-ku, Tokyo 158-8501, Japan

[6]Teijin Institute for Biomedical Research, Asahigaoka 4-3-2, Hino, Tokyo 191-8512, Japan

[7]Institut de Génétique et de Biologie Moleculaire et Cellulaire, Departement of Physiological Genetics / Inserm, U-596 / CNRS, UMR7104 / Université Louis Pasteur, Illkirch, Strasbourg, F-67400 France

[8]St. Vincent's Institute of Medical Research, 9 Princes Street, Fitzroy VIC 3065, Australia

[9]These authors contributed equally to this work.

*Correspondence: uskato@mail.ecc.u-tokyo.ac.jp

DOI 10.1016/j.cell.2007.07.025

SUMMARY

Estrogen prevents osteoporotic bone loss by attenuating bone resorption; however, the molecular basis for this is unknown. Here, we report a critical role for the osteoclastic estrogen receptor α (ERα) in mediating estrogen-dependent bone maintenance in female mice. We selectively ablated ERα in differentiated osteoclasts ($ER\alpha^{\Delta Oc/\Delta Oc}$) and found that $ER\alpha^{\Delta Oc/\Delta Oc}$ females, but not males, exhibited trabecular bone loss, similar to the osteoporotic bone phenotype in postmenopausal women. Further, we show that estrogen induced apoptosis and upregulation of Fas ligand (FasL) expression in osteoclasts of the trabecular bones of WT but not $ER\alpha^{\Delta Oc/\Delta Oc}$ mice. The expression of ERα was also required for the induction of apoptosis by tamoxifen and estrogen in cultured osteoclasts. Our results support a model in which estrogen regulates the life span of mature osteoclasts via the induction of the Fas/FasL system, thereby providing an explanation for the osteoprotective function of estrogen as well as SERMs.

INTRODUCTION

Bone remodeling is a dynamic metabolic process. The destruction or "resorption" of pre-existing bone by mature osteoclasts is followed by the formation of new bone by osteoblasts. Osteoblasts are derived from pleiotropic mesenchymal stem cells in the bone marrow. Mature osteoclasts are multinuclear, macrophage-like cells, derived from hematopoietic stem cells also in the bone marrow. Bone resorption and deposition are tightly coupled, and their balance defines both bone mass as well as quality. The regulation of bone remodeling is complex. A number of systemic hormones and transcription factors directly regulate the proliferation and differentiation of osteoblasts and osteoclasts (Karsenty, 2006; Karsenty and Wagner, 2002; Rodan and Martin, 2000; Teitelbaum and Ross, 2003). Additionally, the indirect cellular communication among groups of bone cells is also physiologically critical for bone growth and remodeling (Martin and Sims, 2005; Mundy and Elefteriou, 2006). The molecular and genetic mechanisms governing bone cell fate have been intensively studied; however, how the life span of bone cells is determined on a molecular level remains elusive.

Estrogen is a key hormone in bone remodeling in several species. The osteoprotective action of estrogen is demonstrable in rodents and is clinically important in humans, particularly older women (Chien and Karsenty, 2005;

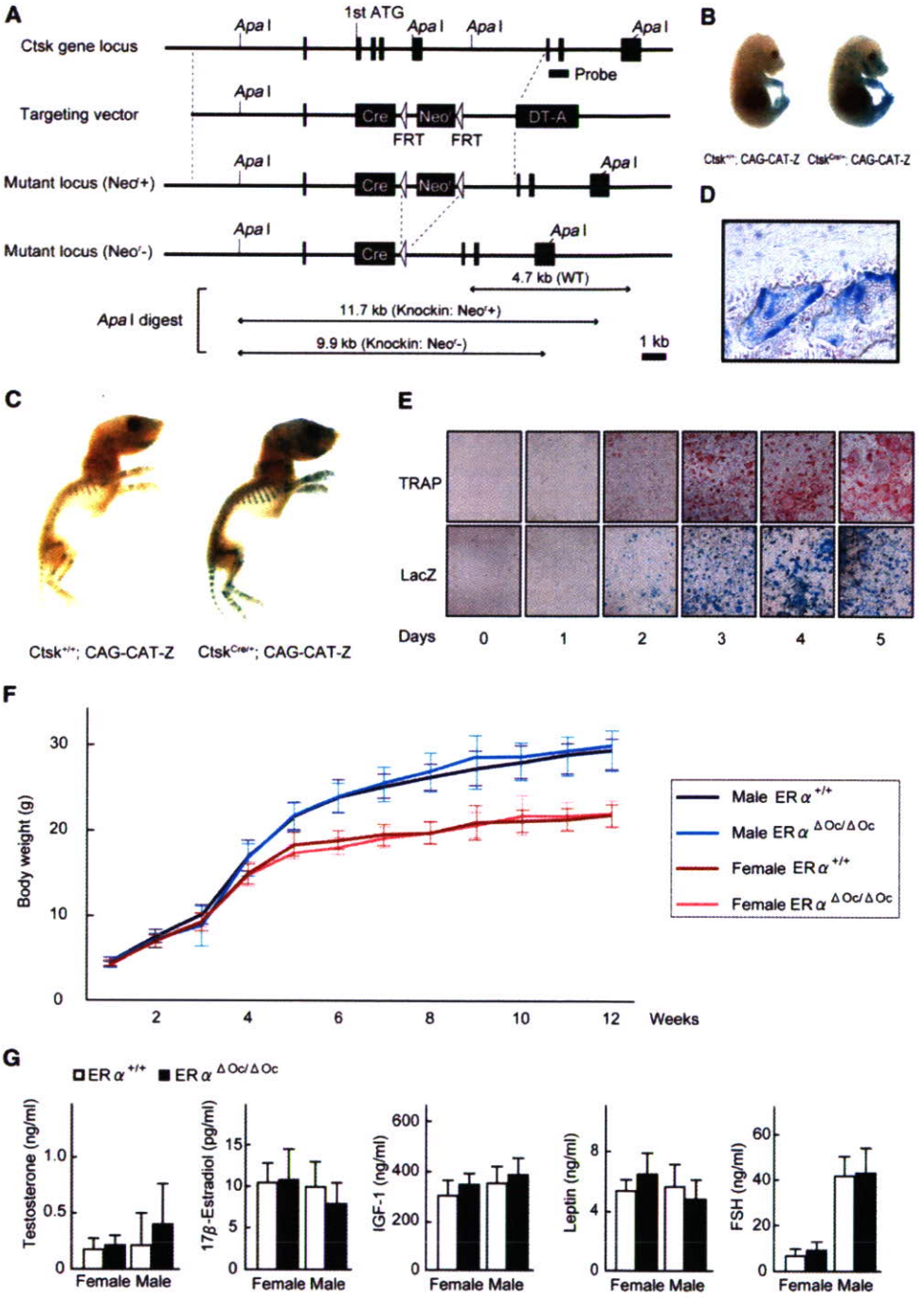

Figure 1. Generation of Knockin Mice Selectively Expressing Cre in Mature Osteoclasts

(A) Illustration of the targeting strategy for insertion of the *Cre* gene into the mouse *Cathepsin K* (*Ctsk*) gene. A targeting vector was generated to contain the *Cre* cDNA at the endogenous ATG start site, followed by a *FRT* (Flp-recombinase target)-flanked *Neo*^{r} cassette. The *DT-A* (diphtheria toxin-A) gene was also inserted to avoid random integrations.

(B and C) *Ctsk-Cre* mice were then crossed with *CAG-CAT-Z* mice. β-galactosidase activity derived from the activated *LacZ* reporter gene was monitored to test if expressed Cre excised the *lox*P sites in mature osteoclasts. LacZ expression patterns reflected the localization patterns of mature osteoclasts in the developing bone at 16.5 days post coitum embryos and in the skeletal tissues of 7-day-old pups.

(D) The LacZ expression induced by Cre-mediated excision was also seen in osteoclasts attached to trabecular bone in the lumber vertebrae of 12-week-old mice.

(E) LacZ expression was induced during osteoclastogenesis. Osteoclast-like cells that differentiated from bone-marrow macrophages following culture in the presence of M-CSF and RANKL were stained with TRAP (tartrate-resistant acid phosphatase), a mature osteoclast marker.

Delmas, 2002; Raisz, 2005; Rodan and Martin, 2000). Estrogen deficiency in postmenopausal women frequently leads to osteoporosis, the most common skeletal disorder. Similarly, ovariectomy clearly produces an osteoporotic bone phenotype in mice. Osteoporotic bone loss is the result of high bone turnover in which bone resorption outpaces bone deposition (Rodan and Martin, 2000; Teitelbaum, 2007). This imbalance in bone turnover that is induced by estrogen deficiency in women and female rodents can be ameliorated with bio-available estrogens including selective estrogen receptor modulators (SERMs) (Riggs and Hartmann, 2003).

Estrogen and SERMs primarily act by regulating gene transcription via estrogen receptors (ERα, ERβ) (Couse and Korach, 1999; Shang and Brown, 2002). ERs belong to the nuclear receptor gene superfamily and act as ligand-inducible transcriptional factors (Mangelsdorf et al., 1995). ER dimers directly or indirectly associate with specific DNA elements in the target gene promoter (Shang and Brown, 2002) and control transcription through reorganizing chromatin structure and histone modifications (Belandia and Parker, 2003). Genetic mouse models (KO mice) lacking ERα ($ER\alpha^{-/-}$) and ERβ ($ER\beta^{-/-}$) provide insights into ER function (Mueller and Korach, 2001; Windahl et al., 2002). In mice, though ERα appears to be the major receptor in most estrogen target tissues including bone (Sims et al., 2003), neither clear bone loss nor high bone turnover is detectable in ERα single or ERα/ERβ double-KO females (Syed and Khosla, 2005; Windahl et al., 2002). This unexpected maintenance of bone mass in female mutants is presumed to be due to unphysiologically elevated levels of other osteoprotective hormones, like androgens. Systemic defects in the hypothalamus caused by ER inactivation appear to impair the negative feedback system of hormone production (Syed and Khosla, 2005). This leads to an excess in estrogen precursors, notably androgens. In fact, the anabolic effects of androgens mediated by the androgen receptor (AR) are evident in female mice (Kawano et al., 2003; Sims et al., 2003). In males, estrogen is also osteoprotective, as is evident by the development of osteopenia in male patients genetically deficient in ERα (Smith et al., 1994) or aromatase activity (Simpson and Davis, 2001). Thus, irrespective of the accumulating clinical and basic research data on the osteoprotective actions of estrogen and SERMs, the molecular basis of this osteoprotection in females remains elusive.

To study the molecular interactions behind the antibone resorptive actions of estrogen in women and female animals, we genetically ablated ERα in mature osteoclasts ($ER\alpha^{\Delta Oc/\Delta Oc}$). Selective ablation of ERα in differentiated osteoclasts ($ER\alpha^{\Delta Oc/\Delta Oc}$) was accomplished by crossing a *Cathepsin K-Cre* knockin mouse with a floxed *ERα* mouse. This resulted in clear trabecular bone loss and high bone turnover associated with increased osteoclast numbers in females but not in males. In the female mutants, further bone loss following ovariectomy was not significant and recovery by estrogen was ineffective in the trabecular areas of long bones and lumbar vertebral bodies. Upregulated expression of *Fas ligand* (*FasL*) gene, and increased apoptosis in differentiated osteoclasts by estrogen was found in the intact bone of wild-type females but undetectable in $ER\alpha^{\Delta Oc/\Delta Oc}$ females. Induction of FasL and apoptosis by estrogen as well as a SERM also required ERα in cultured osteoclasts. Thus, we propose that the osteoprotective actions of estrogen and SERMs are mediated at least in part through osteoclastic ERα in trabecular bone, and the life span of mature osteoclasts is regulated through the activation of the FasL signaling.

RESULTS

Generation of Osteoclast-Specific *ERα* Gene Disruption by Knocked-In *Cre* in the *Cathepsin K* Gene

To specifically disrupt *ERα* gene in mature osteoclasts, we knocked in *Cre* into the gene locus of *Cathepsin K* ($Ctsk^{Cre/+}$) (Figures 1A, S1A, and S1B), a gene known to be expressed in differentiated osteoclastic cells arising from hematopoietic stem cells. This gene is functionally indispensable for mature osteoclasts (Saftig et al., 1998). Only one copy appears enough to support normal bone formation and bone turnover, since heterozygous mutant mice of *Cathepsin K* ($Ctsk^{+/-}$) have no obvious bone phenotype (Gowen et al., 1999; Li et al., 2006; Saftig et al., 1998) . Clear, bone-specific expression of the *Cre* transcript in the adult $Ctsk^{Cre/+}$ mice was observed in the tested tissues (Figure S1C). To confirm Cre protein expression, the $Ctsk^{Cre/+}$ mice were crossed with tester mice (*CAG-CAT-Z*). These mice were genetically engineered to express β-galactosidase by excision of the transcribed stop sequence in front of the *β-galactosidase* gene (*LacZ*) in cells expressing Cre (Sakai and Miyazaki, 1997). β-galactosidase expression visualized by LacZ staining was observed in the bones of 16.5 dpc embryos and 7-day-old pups of $Ctsk^{Cre/+}$; *CAG-CAT-Z* mice. Expression patterns were consistent with the appearance and skeletal localization of functionally mature osteoclasts (Figures 1B and 1C). Histochemical staining of LacZ in the lumbar vertebrae of 12-week-old mice was localized in multinuclear osteoclasts (Figure 1D) but not seen in osteoblasts and osteocytes (Figure S1D) and the hypothalamus (Figure S1E). Since *Cathepsin K* gene expression is evident in differentiated osteoclasts (Saftig et al., 1998), we used an in vitro culture cell system to test whether Cre expression was driven by the endogenous promoter that is induced at the time of osteoclast differentiation. Osteoclast-precursor cells derived from bone marrow

(F) The growth curve of $ER\alpha^{\Delta Oc/\Delta Oc}$ mice was indistinguishable from that of the control mice. Data are represented as mean ± SEM.

(G) Serum hormone levels were normal in 12-week-old $ER\alpha^{\Delta Oc/\Delta Oc}$ (filled column) versus $ER\alpha^{+/+}$ (open column) mice (n = 10–11 animals per genotype). Data are represented as mean ± SEM.

were cytodifferentiated for 1 week in the presence of M-CSF (macrophage colony stimulating factor) and RANKL (receptor activator of NFκB ligand) (Koga et al., 2004). TRAP-positive osteoclasts emerged after 3 days of culture (Figure 1E). The number of TRAP-positive osteoclasts and the number of LacZ-expressing cells simultaneously increased. In the contrast, the LacZ expression was not detected in primary cultured osteoblasts derived from the calvaria (Figure S1F). In view of both our in vivo and in vitro observations, we conclude that the $Ctsk^{Cre/+}$ mouse line expresses Cre in differentiated osteoclasts. Moreover, estrogen response in bone mass control was not distinguishable in between $Ctsk^{Cre/+}$ and $Ctsk^{+/+}$ mice (Figure S2A).

We then crossed floxed $ER\alpha$ mice (Dupont et al., 2000) with $Ctsk^{Cre/+}$ mice to disrupt ERα in differentiated osteoclasts ($ER\alpha^{\Delta Oc/\Delta Oc}$). Excision of the $ER\alpha$ gene (Figure S1G) was confirmed by Southern blotting of DNA from adult female and male (data not shown) bone as well as in cultured mature osteoclasts (Figure S1H). No overt differences were observed in the growth curve, reproduction, or tissues for up to 12 weeks of age (Figure 1F) between the $Ctsk^{Cre/+}$; $ER\alpha^{+/+}$ ($ER\alpha^{+/+}$) and the $Ctsk^{Cre/+}$; $ER\alpha^{flox/flox}$ ($ER\alpha^{\Delta Oc/\Delta Oc}$) mice, with the exception of the female bones. Serum levels of sex hormones and bone remodeling regulators such as IGF-I, leptin, and follicle-stimulating hormone (Sun et al., 2006; Takeda et al., 2002) appeared unchanged in both male and female $ER\alpha^{\Delta Oc/\Delta Oc}$ mice at 12 weeks (Figure 1G).

Osteopenia Occurred in Osteoclast-Specific ERα KO Females But Not Males

The 12-week-old $ER\alpha^{\Delta Oc/\Delta Oc}$ females exhibited a clear reduction in bone mineral density (BMD) in the femurs (Figures 2A–2C) and tibiae (data not shown) when compared with $ER\alpha^{+/+}$ mice. Though cortical bone appeared unaffected, trabecular bone loss (Figure 2A) with significant reduction of trabecular bone volume (BV/TV) (Figure 2F) was clearly seen. This is similar to the osteoporotic abnormalities observed in women during natural menopause or following ovariectomy (Delmas, 2002; Tolar et al., 2004). However, unlike men deficient in aromatase or ERα activity (Simpson and Davis, 2001; Smith et al., 1994), $ER\alpha^{\Delta Oc/\Delta Oc}$ males unexpectedly exhibited no clear bone loss even in the trabecular areas (Figures 2A–2C). In $ER\alpha^{\Delta Oc/\Delta Oc}$ females, both the bone-formation rate, estimated by double-calcein labeling (Figure 2D), as well as the bone-resorption rate, estimated from TRAP-positive differentiated osteoclast numbers (Figure 2E), were increased, indicating high bone turnover. Histomorphometric analyses of $ER\alpha^{\Delta Oc/\Delta Oc}$ females supported the observation of accelerated bone resorption, as increased numbers of osteoclasts (Oc. S/BS and N. Oc/BS) were observed together with more eroded bone surface (ES/BS in Figure 2F). Bone formation was also enhanced as the rates of mineral apposition (MAR) and bone formation (BFR/BS) were both upregulated without an increase in osteoblast numbers (Ob.S/BS) (Figure 2F). Thus, considering all of these findings, it is conceivable that the increased number of differentiated osteoclasts following ERα ablation accelerates bone resorption over formation, leading to bone loss in the trabecular areas.

No Further Bone Loss Results from Estrogen Deficiency in $ER\alpha^{\Delta Oc/\Delta Oc}$ Females

To verify whether osteoclastic ERα indeed mediates osteoprotective estrogen actions, estrogen action was investigated by ovariectomy (OVX) of 12-week-old female mice. As expected, OVX in $ER\alpha^{+/+}$ females resulted in significantly reduced BMD particularly in the trabecular bone (Figures 3A and 3B) but not in the cortical bone (Figure 3C). Consistent with previous reports, (Kimble et al., 1995; Teitelbaum and Ross, 2003), estrogen deficiency following OVX upregulated the serum levels of cytokines like TNFα and IL-1α (Figure 3D). These cytokines enhance bone resorption through stimulation of osteoclastogenesis, leading to the loss of bone mass (Teitelbaum and Ross, 2003). OVX did not further reduce BMD or trabecular bone volume of the femurs of $ER\alpha^{\Delta Oc/\Delta Oc}$ females (Figure 3B) nor affect increased number of TRAP-positive osteoclasts (see lower panel in Figure 3A) despite upregulation of serum cytokines. This suggests that the expression of cytokines known to regulate bone resorption is not under the control of osteoclastic ERα.

Estrogen Treatment Failed to Rescue the Osteoporotic Bone Phenotype of $ER\alpha^{\Delta Oc/\Delta Oc}$ Mice

Estrogen treatment by estrogen pellet implantation (OVX + E2) for 2 weeks after OVX in $ER\alpha^{+/+}$ mice elicited a dramatic increase in bone mass in both the trabecular and cortical areas of the femurs (data not shown) and lumbar vertebral bodies (Figure 4A). Estrogen action during E2 treatment in female mutants ($ER\alpha^{\Delta Oc/\Delta Oc}$) was not as pronounced as in the $ER\alpha^{+/+}$ females (Figures 4A and 4B), and the increase in the trabecular portions of the distal femurs was slight (data not shown). Histomorphometric analysis of the lumbar vertebral bodies (Figure 4B) supported the idea that E2 treatment in the female mutants was not sufficient to suppress accelerated bone resorption. These in vivo findings in the $ER\alpha^{\Delta Oc/\Delta Oc}$ females suggest that in at least the trabecular areas of the long bones and lumbar vertebral bodies, the osteoprotective estrogen action is primarily mediated via osteoclastic ERα inhibiting bone resorption.

To further test this hypothesis, we investigated ERα protein expression in mature osteoclasts from trabecular bone. Few reports document osteoclastic expression of ERα protein and an estrogen response in both intact animals and in in vitro cultured osteoclasts (Bland, 2000). We therefore reasoned that ER expression ceases during differentiation into mature cells from primary cultures of osteoclast precursors, similar to that observed in other primary culture cell systems such as avian oviduct cells, in which ERα protein expression is drastically decreased during culture (Kato et al., 1989). Using highly sensitive immunohistochemistry, we investigated whether

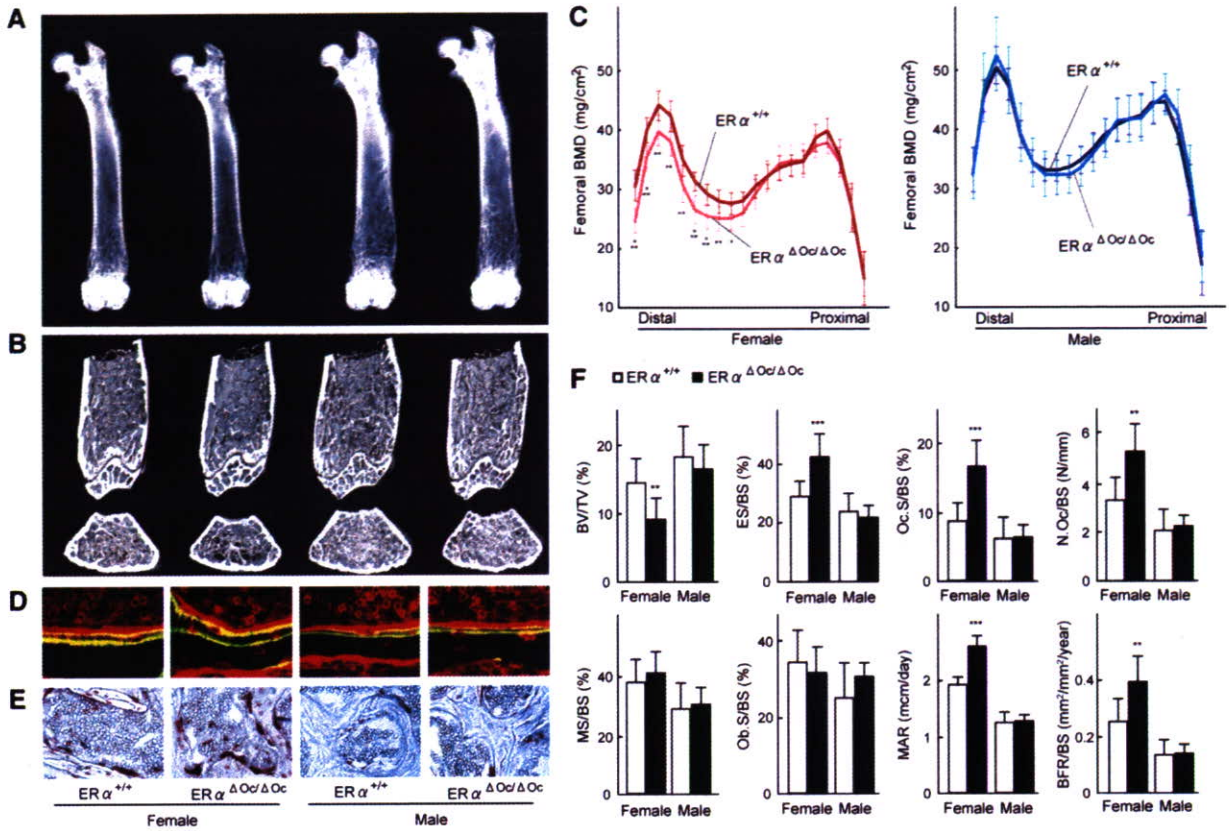

Figure 2. High Bone Turnover Osteopenia Was Observed in $ER\alpha^{\Delta Oc/\Delta Oc}$ Females But Not Males

(A) Soft X-ray images of femurs from 12-week-old $Ctsk^{Cre/+}$; $ER\alpha^{flox/flox}$ ($ER\alpha^{\Delta Oc/\Delta Oc}$) mice.

(B) Three-dimensional computed tomography images of the distal femurs and axial sections of distal metaphysis from representative 12-week-old $Ctsk^{Cre/+}$; $ER\alpha^{+/+}$ ($ER\alpha^{+/+}$) and $ER\alpha^{\Delta Oc/\Delta Oc}$ mice.

(C) BMD of each of 20 equal longitudinal divisions of femurs from 12-week-old $ER\alpha^{+/+}$ and $ER\alpha^{\Delta Oc/\Delta Oc}$ mice. (n = 10–11 animals per genotype; Student's t test, *p < 0.05; **p < 0.01; ***p < 0.001). Data are represented as mean ± SEM.

(D) Bone formation was also accelerated in $ER\alpha^{\Delta Oc/\Delta Oc}$ females when two calcein-labeled mineralized fronts visualized by fluorescent micrography were measured in the proximal tibia of 12-week-old mice.

(E) The number of TRAP-positive osteoclasts in the lumbar spine of female mice was increased by selective disruption of ERα in osteoclasts, indicating enhanced bone resorption.

(F) Bone turnover parameters as measured by dynamic bone histomorphometry after calcein labeling indicated high bone turnover in $ER\alpha^{\Delta Oc/\Delta Oc}$ females. Parameters are measured in the proximal tibia of 12-week-old $ER\alpha^{+/+}$ (open column) and $ER\alpha^{\Delta Oc/\Delta Oc}$ (filled column) mice. BV/TV: bone volume per tissue volume. ES/BS: eroded surface per bone surface. Oc.S/BS: osteoclast surface per bone surface. N.Oc/BS: osteoclast number per bone surface. MS/BS: mineralizing surface per bone surface. Ob.S/BS: osteoblast surface per bone surface. MAR: mineral apposition rate. BFR/BS: bone formation rate per bone surface (n = 10–11 animals per genotype; Student's t test, *p < 0.05; **p < 0.01; ***p < 0.001). Data are represented as mean ± SEM.

ERα protein expresses in differentiated osteoclasts in the bone tissues of femur sections from 12-week-old mice. ERα protein expression appeared abundant in osteoblasts and osteocytes of femur sections (Figure 4C) as well as hypothalamus (Figure S2B) from 12-week-old mice, in agreement with a previous report (Zaman et al., 2006). Likewise, expression levels of ERα in primary cultured osteoblasts derived from calvaria of $ER\alpha^{\Delta Oc/\Delta Oc}$ females appeared unaffected (Figure S2C). In contrast, in differentiated osteoclasts of the same femur sections, ERα expression was definitely detectable but very low in the $ER\alpha^{+/+}$ but undetectable in $ER\alpha^{\Delta Oc/\Delta Oc}$ females (Figure 4C).

Signaling by Osteoclastogenic Factors and Osteoclastogenesis Is Intact in Osteoclasts Deficient in ERα

It is possible that the osteoprotective function of osteoclastic ERα inhibits osteoclastogenesis. To address this issue, osteoclastogenesis was tested in cultured osteoclasts derived from bone-marrow cells of $ER\alpha^{\Delta Oc/\Delta Oc}$ mutants. In this cell culture system, a possible contribution of contaminated immune cells and stromal cells could be excluded, since osteoclastogenesis is only inducible by M-CSF treatment followed by M-CSF + RANKL (Koga et al., 2004).

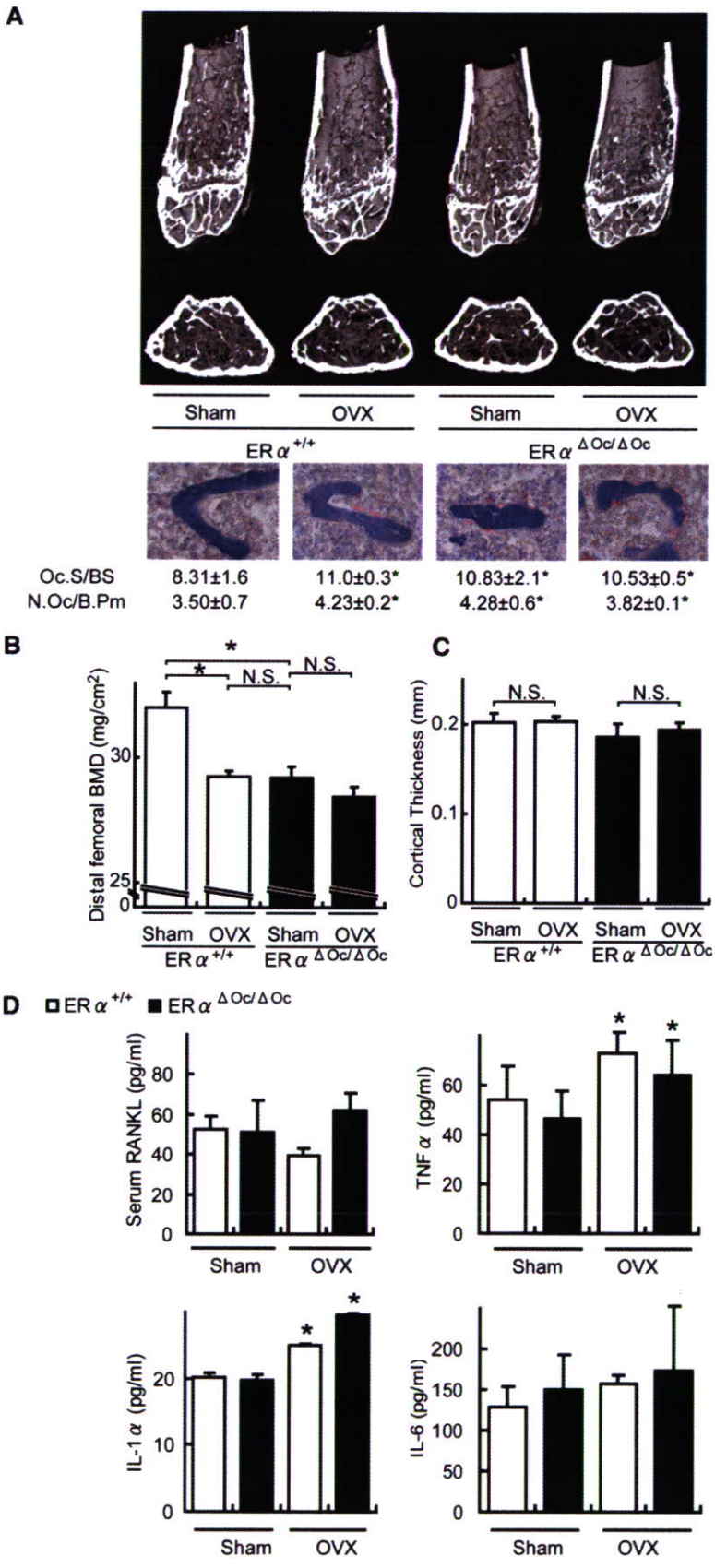

Figure 3. No Further Bone Loss of $ER\alpha^{\Delta Oc/\Delta Oc}$ Females by Ovariectomy

(A) Distal femoral micro CT analysis and lumbar vertebral bone histomorphometrical analysis of sham-operated or ovariectomized (OVX) 12-week-old $ER\alpha^{+/+}$ and $ER\alpha^{\Delta Oc/\Delta Oc}$ mice (*$p < 0.05$ compared to $ER\alpha^{+/+}$ sham group). Two weeks after OVX, the bone phenotype was analyzed.

(B) BMD of the distal femurs within each group are described in Figure 3A (*$p < 0.05$; N.S., not significant). Data are represented as mean ± SEM.

(C) Cortical thickness evaluation from micro CT analysis of femurs within each group described in Figure 3A. Data are represented as mean ± SEM.

(D) The levels of TNFα, IL-1α, and IL-6 in the bone-marrow cells culture media and serum RANKL (*$p < 0.05$ compared to each sham group). Data are represented as mean ± SEM.

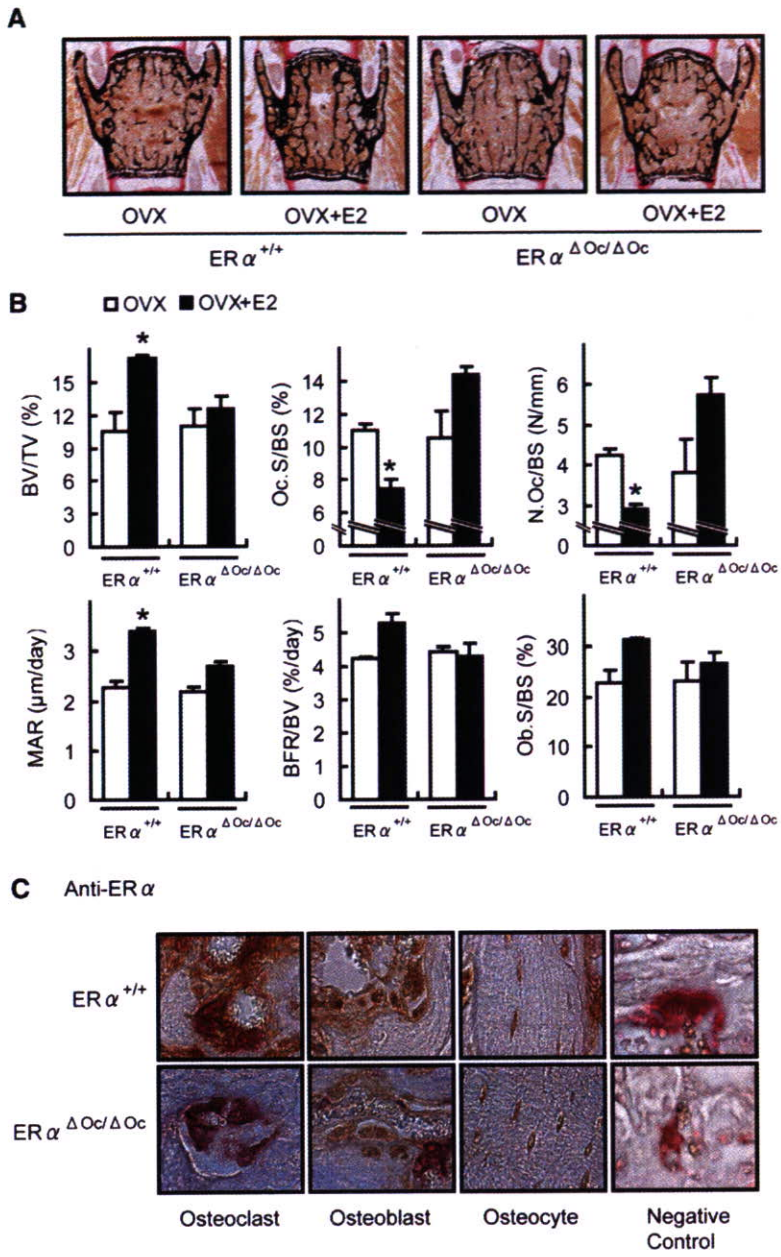

Figure 4. Estrogen treatment failed to reverse trabecular bone loss of ovariectomized $ER\alpha^{\Delta Oc/\Delta Oc}$ females

(A) von kossa staining of lumbar vertebral bodies of ovariectomized $ER\alpha^{+/+}$ and $ER\alpha^{\Delta Oc/\Delta Oc}$ mice treated with or without 17β-estradiol (0.83 μg/day) for 2 weeks (+E2) groups.

(B) Bone histomorphometrical analyses of the lumber vertebral bodies of 12-week-old ovariectomized $ER\alpha^{+/+}$ (left columns) and $ER\alpha^{\Delta Oc/\Delta Oc}$ (right columns) mice with (filled columns) or without (open columns) E2 treatment for 2 weeks (*$p < 0.05$ compared with E2-treated ovariectomized $ER\alpha^{\Delta Oc/\Delta Oc}$ mice). BV/TV: bone volume per tissue volume. ES/BS: eroded surface per bone surface. Oc.S/BS: osteoclast surface per bone surface. N.Oc/BS: osteoclast number per bone surface. MS/BS: mineralizing surface per bone surface. Ob.S/BS: osteoblast surface per bone surface. MAR: mineral apposition rate. BFR/BS: bone formation rate per bone surface. Data are represented as mean ± SEM.

(C) Immunochemical identification of ERα (brown) in TRAP-positive (red) differentiated osteoclasts. The femurs of 12 week-old mice were used for the immunodetection of ERα in bone cells. All labels were abolished when the primary antibody was preadsorbed with the immunizing peptide (negative control).

The number of TRAP-positive osteoclasts differentiated from the bone-marrow cells of $ER\alpha^{\Delta Oc/\Delta Oc}$ females was almost the same as that from $ER\alpha^{+/+}$ females (Figure 5A) and males (data not shown). The differentiated $ER\alpha^{\Delta Oc/\Delta Oc}$ osteoclasts had typical osteoclastic features, including the characteristic cell shape, TRAP-positive, multiple nuclei, and actin-ring formation, and were indistinguishable from the $ER\alpha^{+/+}$ osteoclasts (Figure 5B).

The expression levels of the prime osteoclastogenic transcription factors, c-*fos* and *NFATc1*, were unaltered by ERα deficiency in differentiated osteoclasts (Figure 5C). Furthermore, responses to RANKL in intracellular signaling, as represented by phosphorylation of p38 and IκB, were unaffected in $ER\alpha^{\Delta Oc/\Delta Oc}$ osteoclasts from females (Figure 5D) as well as males (data not shown). In light of these findings, it is unlikely that activated ERα in osteoclastic cells attenuates osteoclastogenesis.

Activation of the Fas/FasL System by Estrogen in Intact Bone Is Impaired by Osteoclastic ERα Deficiency

To examine osteoclastic ERα function in intact bone, DNA microarray analysis following real-time RT-PCR of RNA from the femurs of ovariectomized $ER\alpha^{\Delta Oc/\Delta Oc}$ females treated with or without estrogen, was performed. During

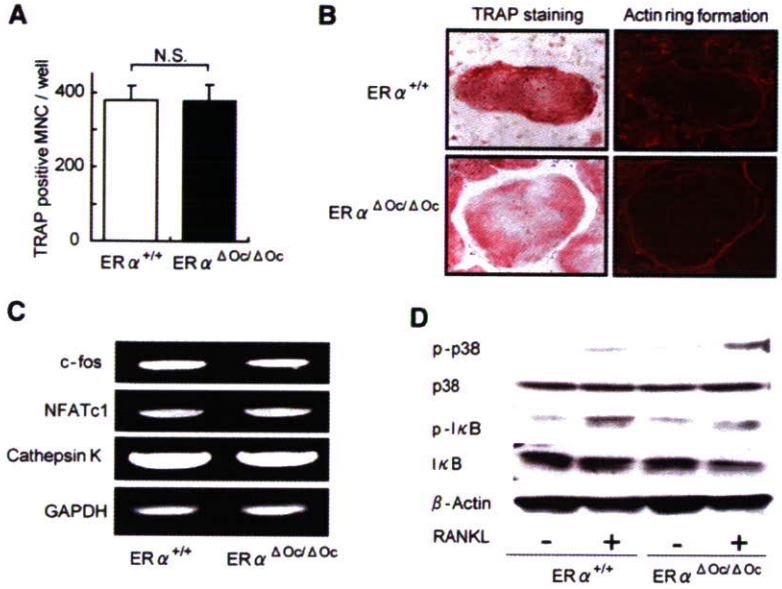

Figure 5. ERα Deficiency Did Not Affect Osteoclastogenesis

(A) TRAP-positive multinucleated cell count at 3 days after RANKL stimulation, cultured in 24-well plates (n = 6, N.S., not significant). Data are represented as mean ± SEM.

(B) TRAP staining and actin ring formation of RANKL induced primary cultured osteoclasts from bone-marrow cells of $ER\alpha^{+/+}$ and $ER\alpha^{\Delta Oc/\Delta Oc}$ mice.

(C) RT-PCR analysis of genes related to osteoclastogenesis.

(D) Western blot analysis of phosphorylated p38, JNK, and IκB of primary cultured bone-marrow cells stimulated with or without 100 ng/ml of RANKL for 15 min.

the search for candidate ERα target genes in bone by DNA microarray analysis (Figure S3), we found that a number of apoptosis-related factors were regulated by estrogen in the intact bone of $ER\alpha^{+/+}$ females but dysregulated in $ER\alpha^{\Delta Oc/\Delta Oc}$ females. This observation is consistent with a previous report of estrogen-induced apoptosis of mature osteoclasts (Kameda et al., 1997). Real-time RT-PCR to validate the estrogen regulations of the candidate genes revealed that gene expression of *FasL*, an apoptotic factor, was responsive to E2 (Figure 6A). Estrogen treatment (+E2) indeed induced expression of FasL protein in bone of ovariectomized $ER\alpha^{+/+}$, but this induction was not obvious in ovariectomized $ER\alpha^{\Delta Oc/\Delta Oc}$ mice (Figures 6B and 6C). Reflecting FasL induction by estrogen, estrogen-induced apoptosis (as observed by the TUNEL assay) in TRAP-positive mature trabecular osteoclasts in the distal femurs of the $ER\alpha^{+/+}$ mice was detected, but this E2 response was abolished in the $ER\alpha^{\Delta Oc/\Delta Oc}$ mice (Figure 6D). Furthermore, in mice lacking functional FasL ($FasL^{gld/gld}$), neither enhanced bone resorption nor bone mass loss was induced by ovariectomy (Figures 6E and 6F).

Osteoclastic ERα Mediates Estrogen-Induced apoptosis by FasL

The expression level of ERα protein in differentiated osteoclasts derived from bone marrow cells was very low, but induction of *FasL* gene expression was also detectable in the cultured osteoclasts of $ER\alpha^{+/+}$ females as well as males (Figure 7A). However, this E2 response was impaired in cultured osteoclasts from $ER\alpha^{\Delta Oc/\Delta Oc}$ females (Figure 7A). It is notable that such responses are also induced by tamoxifen (Figure 7C), which is an osteoprotective SERM (Harada and Rodan, 2003). ERα overexpression augmented *FasL* gene expression in response to estrogen in cultured osteoclasts from $ER\alpha^{\Delta Oc/\Delta Oc}$ females (Figure S4A). In primary cultured calvarial osteoblasts from females as well as males (Suzawa et al., 2003), *FasL* gene induction by E2 and tamoxifen was also seen; however, it was not accompanied by increased apoptosis (data not shown). Thus, it appears that estrogen-induced apoptosis in osteoclasts is mediated by FasL expression in osteoclasts in the trabecular bone areas, presumably as well as in osteoblasts in cortical bone areas. As expected, the cell number of TUNEL-positive osteoclasts was increased by E2 in the cultured osteoclasts from $ER\alpha^{+/+}$ females, but E2-induced apoptosis was undetectable in $ER\alpha^{\Delta Oc/\Delta Oc}$ osteoclasts (Figure 7B). Consistent with FasL-induced apoptosis, *Fas* gene expression was observed (Figure 7D), but it was likely that Fas expression did not require ERα function (Figures S4B and S4C). Expression levels of *Fas* and *ERα* as well as E2 response in apoptosis appeared to fluctuate during osteoclast differentiation (Figures S4B–S4D); however, in FasL mutant ($FasL^{gld/gld}$) females, the E2-induced apoptosis was abolished (Figure S4E). These findings suggest that activated ERα in differentiated osteoclasts induces apoptosis through activating FasL/Fas signaling. This leads to suppression of bone resorption through truncating the already short life span of differentiated osteoclasts (Teitelbaum, 2006).

DISCUSSION

Selective ablation of ERα in mature osteoclasts in female mice shows that the osteoprotective effect of estrogen is mediated by osteoclastic ERα, at least in the trabecular regions of the tibiae, femur, and lumbar vertebrae of female mice. Activated ERα by estrogen as well as SERMs appears to truncate the already short life span (estimated at 2 weeks) of differentiated osteoclasts by inducing apoptosis through activation of the Fas/FasL system.

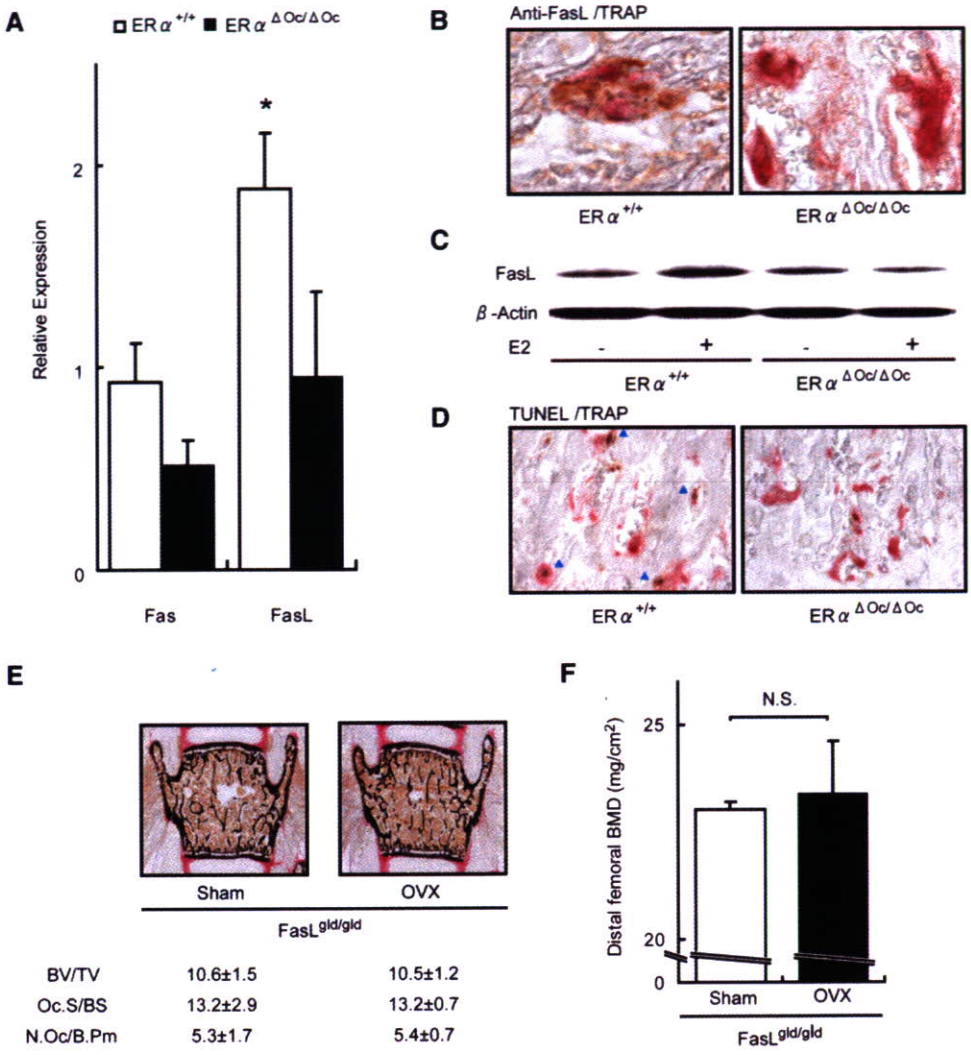

Figure 6. Activated ERα Induced Fas Ligand Expression and Apoptosis in Differentiated Osteoclasts of Intact Bone

(A) Real-time RT-PCR analysis of *Fas* and *FasL*. Expression levels in bones from E2-treated ovariectomized $ER\alpha^{+/+}$ (open column) and $ER\alpha^{\Delta Oc/\Delta Oc}$ (filled column) were compared with the ovariectomized groups of each genotype without E2 administration (*$p < 0.05$ compared to $ER\alpha^{+/+}$). Data are represented as mean ± SEM.

(B) Immunohistochemical analysis of anti-FasL with TRAP staining of the sections from the distal femurs of E2-treated ovariectomized $ER\alpha^{+/+}$ and $ER\alpha^{\Delta Oc/\Delta Oc}$ mice. Brawny stained cells are anti-FasL positive.

(C) Anti-FasL western blot analysis of proteins obtained from femurs of ovariectomized $ER\alpha^{+/+}$ and $ER\alpha^{\Delta Oc/\Delta Oc}$ mice treated with or without E2, using anti-β-actin as internal control.

(D) TUNEL staining with TRAP staining of the sections from the distal femurs of E2-treated ovariectomized $ER\alpha^{+/+}$ and $ER\alpha^{\Delta Oc/\Delta Oc}$ mice. Arrowheads indicate both TUNEL (brown)- and TRAP-positive staining cells.

(E) Bone histomorphometrical analysis of sham-operated or ovariectomized $FasL^{gld/gld}$ mice.

(F) BMD of the distal femurs of sham operated or ovariectomized $FasL^{gld/gld}$ mice. Data are represented as mean ± SEM.

This attenuates bone resorption. This idea is supported by previous observations that estrogen deficiency following menopause or ovariectomy leads to high bone turnover, particularly in the trabecular areas, as bone is rapidly lost through enhanced resorption (Delmas, 2002; Tolar et al., 2004). Thus, estrogen treatment leads to recovery from osteopenia by reducing resorption (Delmas, 2002; Rodan and Martin, 2000), partly by the induction of osteoclast cell death.

In contrast to the osteopenia seen in the $ER\alpha^{\Delta Oc/\Delta Oc}$ females, the $ER\alpha^{\Delta Oc/\Delta Oc}$ male mice unexpectedly had no bone loss. The male mice still demonstrated an ERα-mediated induction of FasL in response to estrogen with subsequent apoptosis of osteoclasts (Figure 7). Both male mice with a deficiency of aromatase that are unable to locally produce estrogen from testosterone and men with a genetic mutation in the *ERα* gene suffer from osteoporosis (Smith et al., 1994). Considering that the

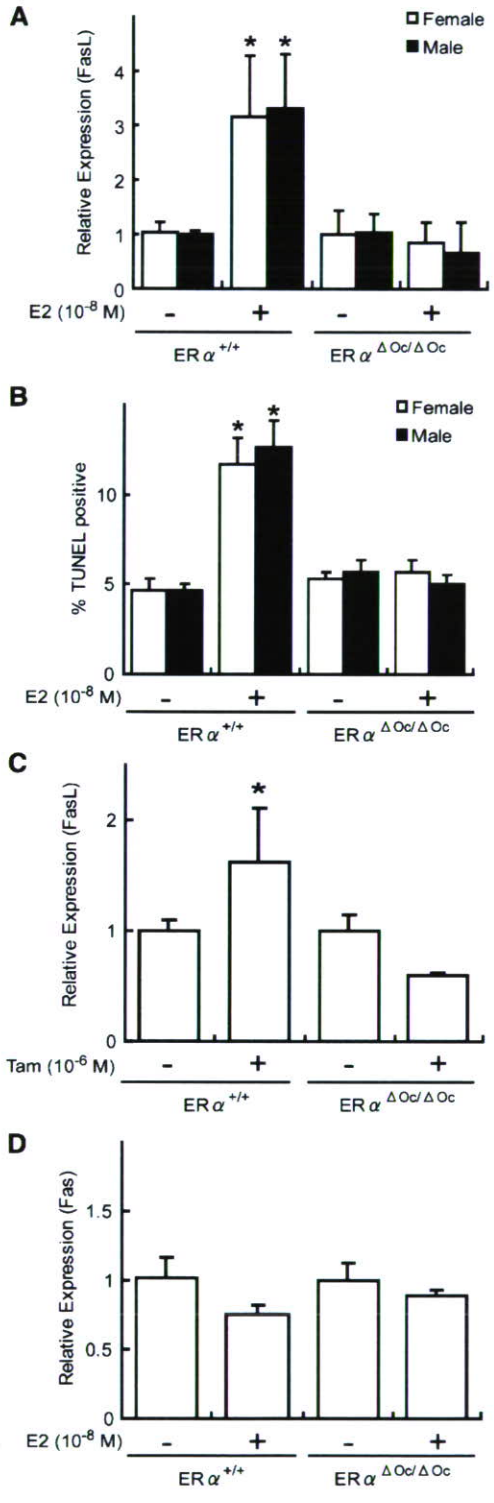

Figure 7. Estrogen-Induced *FasL* Expression and Apoptosis Required ERα in Cultured Osteoclasts

(A) Real-time RT-PCR analysis of *FasL* expression using total RNA obtained from in vitro primary cultured osteoclasts of each genotype at 3 days after RANKL stimulation, treated with or without E2 (10^{-8} M) for 4 hr (*$p < 0.05$ compared to the group treated without E2). Data are represented as mean ± SEM.

(B) Apoptotic cells were defined as those with TUNEL-positive nuclei among TRAP-positive multinucleated primary cultured osteoclasts treated with or without E2 (10^{-8} M) for 12 hr in 96-well plates (*$p < 0.05$ compared to the group treated without E2). Data are represented as mean ± SEM.

(C) *FasL* expression in each genotypic female osteoclastic cells treated with or without Tam (10^{-6} M) (*$p < 0.05$ compared to the group treated without Tam). Data are represented as mean ± SEM.

(D) Expression of *Fas* was measured as described in the legend of Figure 7A. Data are represented as mean ± SEM.

markedly elevated levels of testosterone in ERα KO females may be potent enough to maintain normal bone turnover (Syed and Khosla, 2005), it is likely that the activated AR might be functionally sufficient in male mice to compensate for the ERα deficiency in bone (Kawano et al., 2003). However, species differences in the osteoprotective action of sex steroid hormones still need to be carefully addressed.

Fas/FasL system-mediated apoptotic induction of osteoclasts by estrogen may well be a part of the mechanism for the antiresorptive action of estrogen and SERMs in trabecular bone areas (Delmas, 2002; Rodan and Martin, 2000; Simpson and Davis, 2001; Syed and Khosla, 2005; Tolar et al., 2004). Regulation of osteoclast differentiation is tightly coupled to osteoblastic function in terms of cytokine production and cell-cell contact (Karsenty and Wagner, 2002; Martin and Sims, 2005; Mundy and Elefteriou, 2006; Teitelbaum and Ross, 2003). Indeed, upregulation of osteoclastogenic cytokines by ovariectomy was unaffected in $ER\alpha^{\Delta Oc/\Delta Oc}$ females. Considering the observation that cortical bone mass is increased in ovariectomized $ER\alpha^{\Delta Oc/\Delta Oc}$ females during estrogen treatment, it is conceivable that the antiresorptive estrogen action in cortical bone is also mediated by osteoblastic ERα. In this regard, FasL induction by estrogen in osteoblasts may contribute to the osteoprotective estrogen action, and *FasL* gene induction by estrogen was in fact detected in primary cultured osteoblasts from female calvaria by us as well as another group (S. Krum and M. Brown, personal communication). Thus, similar experiments in which ERα is selectively ablated in osteoblasts are needed to define the role of ERα in these cells.

In osteoclastic cells, expression of the *FasL* gene, which leads to apoptosis, appears to be positive controlled by activated ERα. Not surprisingly, a direct binding site for ERα has been mapped in the *FasL* gene locus (S. Krum and M. Brown, personal communication). An osteoclast- and cell-differentiation stage-specific mechanism may underlie this gene induction in the *FasL* gene promoter. A recent study demonstrated that ERα recruitment to specific promoter sites of given ERα target genes was cell-type specific (Carroll et al., 2005). Thus, there is significant impetus to identify the osteoclastic factor that associates with ERα in the *FasL* gene promoter. Such identification will lead to a better understanding of the molecular basis of the osteoprotective estrogen action and provide a target against which to develop SERMs of greater effectiveness.

EXPERIMENTAL PROCEDURES

Ctsk-Cre Construction and Generation of the Knockin Mouse Lines

An RP23-422n18 BAC clone containing the mouse *Ctsk* gene was purchased from Invitrogen (Carlsbad, CA). The *FRT-Kan^r/Neo^r-FRT* and *nlsCre* fragments were obtained from plasmids pSK2/3-*FRT-Neo* and pIC-*Cre*. Two homologous arms of 500 bp from the *Ctsk* gene were inserted into both sides of the *nlsCre-FRT-Kan^r/Neo^r-FRT* cassette in the pSK2/3-*FRT-Neo* plasmid. The *nlsCre-FRT-Kan^r/Neo^r-FRT* cassette was introduced into the endogenous ATG start site of the *Ctsk* gene by recombineering approaches (Copeland et al., 2001). Targeted BAC was reduced in size from 189 kb to 26 kb and subcloned into the pMC1-DTpA vector by the gap-repair method. The targeted TT2 ES clones were selected after positive-negative selection with G418 and DT-A with Southern analysis, then aggregated with single eight-cell embryos from CD-1 mice (Yoshizawa et al., 1997). Chimeric mice were then crossed with a general deleter mouse line, *ACTB-Flpe* (Jackson Laboratory), to remove the *Kan^r/Neo^r* cassette. The *Ctsk-Cre* mice (*Ctsk$^{Cre/+}$*), originally on a hybrid C57BL/6 and CBA genetic background, were backcrossed for four generations into a C57BL/6J background. *FasL$^{gld/gld}$* mice were also purchased from Jackson Laboratory.

Analysis of Cre Recombinase Activities

Expression of the Cre transcript was detected by RT-PCR. Southern analysis using a *Cre* cDNA probe was performed with total RNA extracted from 12-week-old mice. To evaluate the specificity and efficiency of Cre-mediated recombination, we mated the *Ctsk$^{Cre/+}$* mice to *CAG-CAT-Z* reporter mice (kindly provided by J. Miyazaki) (Sakai and Miyazaki, 1997) and genotyped their offspring with *Cre*-specific primers. β-galactosidase activity of the expressed *LacZ* gene driven by the *CAG* promoter was expected to be detected in the given cells expressing functional Cre recombinase.

In Vitro Osteoclastogenesis and Ligand Application

Bone-marrow cells derived from 8-week-old mice were plated in culture dishes containing α-MEM (GIBCO-BRL) with 10% FBS (JRH) and 10 ng/ml M-CSF (Genzyme). After incubation for 48 hr, adherent cells were used as osteoclast precursor cells after washing out the nonadherent cells. Cells were cultured in the presence of 10 ng/ml M-CSF and 100 ng/ml RANKL (Peprotech) to generate osteoclast-like cells (Koga et al., 2004) for 3 days, so the total culture time was 5 days. Three days after RANKL stimulation, primary cultured osteoclasts were treated with 10^{-8} M of 17β-estradiol (E2) (Sigma-Aldrich Co.) or 10^{-6} M 4-hydroxytamoxifen (Tam) (Sigma-Aldrich Co.) in phenol-red free medium.

Generation of Osteoclast-Specific ERα KO Mice

The ERα conditional (*ERα$^{flox/flox}$*) (Dupont et al., 2000) and null alleles with a C57BL/6J background have been previously described. *ERα$^{flox/flox}$* mice were crossed with *Ctsk$^{Cre/+}$* mice to generate *Ctsk$^{Cre/+}$; ERα$^{flox/+}$* mice. *Ctsk$^{Cre/+}$; ERα$^{+/+}$* (*ERα$^{+/+}$*) and *Ctsk$^{Cre/+}$; ERα$^{flox/flox}$* (*ERα$^{\Delta Oc/\Delta Oc}$*) mice were obtained by crossing *Ctsk$^{Cre/+}$; ERα$^{flox/+}$* with *ERα$^{flox/+}$* mouse lines.

Radiological Analysis

Bone radiographs of the femurs of 12-week-old *Ctsk$^{Cre/+}$; ERα$^{flox/flox}$* (*ERα$^{\Delta Oc/\Delta Oc}$*) and *Ctsk$^{Cre/+}$; ERα$^{+/+}$* (*ERα$^{+/+}$*) littermates were visualized with a soft X-ray apparatus (TRS-1005: SOFTRON). BMD was measured by DXA using a bone mineral analyzer (DCS-600EX: ALOKA). Micro Computed Tomography scanning of the femurs was performed using a composite X-ray analyzer (NX-CP-C80H-IL: Nittetsu ELEX Co.) (Kawano et al., 2003). Tomograms were obtained with a slice thickness of 10 μm and reconstructed at 12 × 12 pixels into a 3D image by the volume-rending method (VIP-Station; Teijin System Technology) using a computer.

Analysis of Skeletal Morphology

Twelve-week-old *Ctsk$^{Cre/+}$; ERα$^{flox/flox}$* (*ERα$^{\Delta Oc/\Delta Oc}$*) and *Ctsk$^{Cre/+}$; ERα$^{+/+}$* (*ERα$^{+/+}$*) littermates were double labeled with subcutaneous injections of 16 mg/kg of calcein (Sigma) at 4 and 2 days before sacrifice. Tibiae were removed from each mouse and fixed with 70% ethanol. They were stained with Villanueva bone stain for 7 days and embedded in methyl-methacrylate (Wako) (Yoshizawa et al., 1997). Frontal plane sections (5-μm thick) of the proximal tibia were cut using a Microtome (LEICA). The cancellous bone was measured in the secondary spongiosa located 500 μm from the epiphyseal growth plate and 160 μm from the endocortical surface (Kawano et al., 2003; Nakamichi et al., 2003). Bone histomorphometric measurements of the tibia were made using a semiautomatic image analyzing system (System Supply) and a fluorescent microscope (Optiphot; Nikon). Similar measurements of the lumbar vertebral bodies were done as previously reported (Takeda et al., 2002). Standard bone histomorphometrical nomenclatures, symbols, and units were used as described in the report of the ASBMR Histomophometry Nomenclature Committee.

Ovariectomy and Hormone Replacement

Female *Ctsk$^{Cre/+}$; ERα$^{flox/flox}$* (*ERα$^{\Delta Oc/\Delta Oc}$*) and *Ctsk$^{Cre/+}$; ERα$^{+/+}$* (*ERα$^{+/+}$*) littermates were ovariectomized or sham operated at 8–12 weeks of age for 2 weeks for all experiments, and slow releasing pellets of E2 (0.83 μg/day) or placebo (Innovative Research, Sarasota, FL) were implanted subcutaneously in the scapular region behind the neck (Sato et al., 2004; Shiina et al., 2006).

Immunohistochemistry

Twelve-week-old *Ctsk$^{Cre/+}$; ERα$^{flox/flox}$* (*ERα$^{\Delta Oc/\Delta Oc}$*) and *Ctsk$^{Cre/+}$; ERα$^{+/+}$* (*ERα$^{+/+}$*) littermates were fixed with 4% PFA by perfusion. Serial sections of the brain (20 μm thick) were divided into two groups and used for single labeling for the ERα or thionin to allow determination of the areas to be measured. Tibiae and femurs were decalcified in 10% EDTA for 2–4 weeks after fixation and then embedded in paraffin sections. Sections were incubated in L.A.B. solution (Polysciences) for 30 min to retrieve antigen. The cooled sections were incubated in 1% H_2O_2 for 30 min to quench endogenous peroxidase and then washed with 1% Triton X-100 in PBS for 10 min. To block nonspecific antibody binding, sections were incubated in blocking solution (DAKO) for 5 min. Sections were then incubated with anti-ERα (Santa Cruz, CA) and anti-FasL (Santa Cruz, CA) in blocking solution overnight at 4°C. Staining was then performed using the EnVision+ HRP System (Dako) and 3, 3′-diaminobendizine tetrahydrochloride substrate (Sigma), counterstained with TRAP, dehydrated through an ethanol series and xylene, before mounting (Sato et al., 2004).

ERα Overexpression

Two days after RANKL stimulation, an expression vector of mouse ERα was tranfected into immature osteoclastic cells from *ERα$^{\Delta Oc/\Delta Oc}$* mice using Superfect (QIAGEN) as manufacture's instruction.

Real-Time RT-PCR

One microgram of total RNA from each sample was reverse transcribed into first-strand cDNA with random hexamers using Superscript III reverse transcriptase (Invitrogen). Primer sets for all genes were purchased from Takara Bio. Inc. (Tokyo, Japan). Real-time RT-PCR was performed using SYBR Premix Ex Taq (Takara) with the ABI PRISM 7900HT (Applied Biosystems) according to the manufacturer's instructions. Experimental samples were matched to a standard curve generated by amplifying serially diluted products using the same PCR protocol. To correct for variability in RNA recovery and efficiency of reverse transcription, *Gapdh* cDNA was amplified and quantified in each cDNA preparation. Normalization and calculation steps were performed as reported previously (Takezawa et al., 2007).

TUNEL/TRAP Staining

The TUNEL method was performed using the ApopTag Fluorescein In Situ Apoptosis Detection Kit (CHEMICON international) according to the manufacturer's instructions with a slight modification. This was followed by TRAP staining as previously reported (Kobayashi et al., 2000).

Cytokine Assays

Bone marrow and blood were collected at 2 weeks after sham operation or ovariectomy. Bone-marrow cells were cultured for 3 days in DMEM. The levels of TNFα, IL-1α, and IL-6 in the culture media and serum RANKL were determined by ELISA (R&D Systems).

Western Blot

Osteoclast precursor cells were treated with or without 100 ng/ml of soluble RANKL. After 15 minutes, cell extracts were harvested from the cells using lysis buffer containing 100 mM Tris-HCl (pH 7.8), 150 mM NaCl, 0.1% Triton X-100, 5% protease inhibitor cocktail (Sigma), and 5% phosphatase inhibitor cocktail (Sigma). An equivalent amount of protein from each of the cell extracts and proteins of femoral bone extracted using ISOGEN was loaded for SDS-PAGE and transferred to PVDF membranes (Amersham Biosciences). The membranes were developed with enhanced chemiluminescence reagent (Amersham Biosciences) (Ohtake et al., 2003). Phosphorylation of p38 MAPK and IκB were evaluated using antibodies purchased from Cell Signaling Technology (Koga et al., 2004) and anti-FasL antibody was purchased from Santa Cruz Biotechnology (sc-834).

Actin-Ring Formation

Cells were fixed for 15 min in warm 4% paraformaldehyde (PFA). After fixation, cells were washed three times with PBS with 0.1% Triton X-100 (PBST) and incubated with 0.2 U/ml rhodamine phalloidin (Molecular Probes) for 30 min and washed again three times in PBST.

Statistical Analysis

Data were analyzed by two-tailed student's t test. For all graphs, data are represented as mean ± SEM.

Supplemental Data

Supplemental Data include Supplemental Experimental Procedures and four figures and can be found with this article online at http://www.cell.com/cgi/content/full/130/5/811/DC1/.

ACKNOWLEDGMENTS

We thank Drs. S. Krum and M. Brown to share with their unpublished results; Drs. K. Yoshimura, Y. Nakamichi, T. Watanabe, J. Miyamoto, H. Shiina, T. Fukuda, Ms. Y. Sato, and S. Tanaka for generation of the KO mice; Drs. T. Koga, H. Takagi, E. Ochiai, and N. Moriyama for technical help; Dr. J. Miyazaki for *CAG-CAT-Z* reporter mice, and H. Higuchi and K. Hiraga for manuscript preparation. This work was supported in part by priority areas from the Ministry of Education, Culture, Sports, Science and Technology (to S.K.) and the Program for Promotion of Basic Research Activities for Innovative Biosciences (PROBRAIN).

Received: February 23, 2007
Revised: May 21, 2007
Accepted: July 17, 2007
Published: September 6, 2007

REFERENCES

Belandia, B., and Parker, M.G. (2003). Nuclear receptors: a rendezvous for chromatin remodeling factors. Cell *114*, 277–280.

Bland, R. (2000). Steroid hormone receptor expression and action in bone. Clin. Sci. (Lond.) *98*, 217–240.

Carroll, J.S., Liu, X.S., Brodsky, A.S., Li, W., Meyer, C.A., Szary, A.J., Eeckhoute, J., Shao, W., Hestermann, E.V., Geistlinger, T.R., et al. (2005). Chromosome-wide mapping of estrogen receptor binding reveals long-range regulation requiring the forkhead protein FoxA1. Cell *122*, 33–43.

Chien, K.R., and Karsenty, G. (2005). Longevity and lineages: toward the integrative biology of degenerative diseases in heart, muscle, and bone. Cell *120*, 533–544.

Copeland, N.G., Jenkins, N.A., and Court, D.L. (2001). Recombineering: a powerful new tool for mouse functional genomics. Nat. Rev. Genet. *2*, 769–779.

Couse, J.F., and Korach, K.S. (1999). Estrogen receptor null mice: what have we learned and where will they lead us? Endocr. Rev. *20*, 358–417.

Delmas, P.D. (2002). Treatment of postmenopausal osteoporosis. Lancet *359*, 2018–2026.

Dupont, S., Krust, A., Gansmuller, A., Dierich, A., Chambon, P., and Mark, M. (2000). Effect of single and compound knockouts of estrogen receptors alpha (ERalpha) and beta (ERbeta) on mouse reproductive phenotypes. Development *127*, 4277–4291.

Gowen, M., Lazner, F., Dodds, R., Kapadia, R., Feild, J., Tavaria, M., Bertoncello, I., Drake, F., Zavarselk, S., Tellis, I., et al. (1999). Cathepsin K knockout mice develop osteopetrosis due to a deficit in matrix degradation but not demineralization. J. Bone Miner. Res. *14*, 1654–1663.

Harada, S., and Rodan, G.A. (2003). Control of osteoblast function and regulation of bone mass. Nature *423*, 349–355.

Kameda, T., Mano, H., Yuasa, T., Mori, Y., Miyazawa, K., Shiokawa, M., Nakamaru, Y., Hiroi, E., Hiura, K., Kameda, A., et al. (1997). Estrogen inhibits bone resorption by directly inducing apoptosis of the bone-resorbing osteoclasts. J. Exp. Med. *186*, 489–495.

Karsenty, G. (2006). Convergence between bone and energy homeostases: leptin regulation of bone mass. Cell Metab. *4*, 341–348.

Karsenty, G., and Wagner, E.F. (2002). Reaching a genetic and molecular understanding of skeletal development. Dev. Cell *2*, 389–406.

Kato, S., Ito, S., Noguchi, T., and Naito, H. (1989). Effects of brefeldin A on the synthesis and secretion of egg white proteins in primary cultured oviduct cells of laying Japanese quail (Coturnix coturnix japonica). Biochim. Biophys. Acta *991*, 36–43.

Kawano, H., Sato, T., Yamada, T., Matsumoto, T., Sekine, K., Watanabe, T., Nakamura, T., Fukuda, T., Yoshimura, K., Yoshizawa, T., et al. (2003). Suppressive function of androgen receptor in bone resorption. Proc. Natl. Acad. Sci. USA *100*, 9416–9421.

Kimble, R.B., Matayoshi, A.B., Vannice, J.L., Kung, V.T., Williams, C., and Pacifici, R. (1995). Simultaneous block of interleukin-1 and tumor necrosis factor is required to completely prevent bone loss in the early postovariectomy period. Endocrinology *136*, 3054–3061.

Kobayashi, Y., Hashimoto, F., Miyamoto, H., Kanaoka, K., Miyazaki-Kawashita, Y., Nakashima, T., Shibata, M., Kobayashi, K., Kato, Y., and Sakai, H. (2000). Force-induced osteoclast apoptosis in vivo is accompanied by elevation in transforming growth factor beta and osteoprotegerin expression. J. Bone Miner. Res. *15*, 1924–1934.

Koga, T., Inui, M., Inoue, K., Kim, S., Suematsu, A., Kobayashi, E., Iwata, T., Ohnishi, H., Matozaki, T., Kodama, T., et al. (2004). Costimulatory signals mediated by the ITAM motif cooperate with RANKL for bone homeostasis. Nature *428*, 758–763.

Li, C.Y., Jepsen, K.J., Majeska, R.J., Zhang, J., Ni, R., Gelb, B.D., and Schaffler, M.B. (2006). Mice lacking Cathepsin K maintain bone remodeling but develop bone fragility despite high bone mass. J. Bone Miner. Res. *21*, 865–875.

Mangelsdorf, D.J., Thummel, C., Beato, M., Herrlich, P., Schutz, G., Umesono, K., Blumberg, B., Kastner, P., Mark, M., Chambon, P., and Evans, R.M. (1995). The nuclear receptor superfamily: the second decade. Cell *83*, 835–839.

Martin, T.J., and Sims, N.A. (2005). Osteoclast-derived activity in the coupling of bone formation to resorption. Trends Mol. Med. *11*, 76–81.

Mueller, S.O., and Korach, K.S. (2001). Estrogen receptors and endocrine diseases: lessons from estrogen receptor knockout mice. Curr. Opin. Pharmacol. *1*, 613–619.

Mundy, G.R., and Elefteriou, F. (2006). Boning up on ephrin signaling. Cell *126*, 441–443.

Nakamichi, Y., Shukunami, C., Yamada, T., Aihara, K., Kawano, H., Sato, T., Nishizaki, Y., Yamamoto, Y., Shindo, M., Yoshimura, K., et al. (2003). Chondromodulin I is a bone remodeling factor. Mol. Cell. Biol. *23*, 636–644.

Ohtake, F., Takeyama, K., Matsumoto, T., Kitagawa, H., Yamamoto, Y., Nohara, K., Tohyama, C., Krust, A., Mimura, J., Chambon, P., et al. (2003). Modulation of oestrogen receptor signalling by association with the activated dioxin receptor. Nature *423*, 545–550.

Raisz, L.G. (2005). Pathogenesis of osteoporosis: concepts, conflicts, and prospects. J. Clin. Invest. *115*, 3318–3325.

Riggs, B.L., and Hartmann, L.C. (2003). Selective estrogen-receptor modulators–mechanisms of action and application to clinical practice. N. Engl. J. Med. *348*, 618–629.

Rodan, G.A., and Martin, T.J. (2000). Therapeutic approaches to bone diseases. Science *289*, 1508–1514.

Saftig, P., Hunziker, E., Wehmeyer, O., Jones, S., Boyde, A., Rommerskirch, W., Moritz, J.D., Schu, P., and von Figura, K. (1998). Impaired osteoclastic bone resorption leads to osteopetrosis in Cathepsin-K-deficient mice. Proc. Natl. Acad. Sci. USA *95*, 13453–13458.

Sakai, K., and Miyazaki, J. (1997). A transgenic mouse line that retains Cre recombinase activity in mature oocytes irrespective of the cre transgene transmission. Biochem. Biophys. Res. Commun. *237*, 318–324.

Sato, T., Matsumoto, T., Kawano, H., Watanabe, T., Uematsu, Y., Sekine, K., Fukuda, T., Aihara, K., Krust, A., Yamada, T., et al. (2004). Brain masculinization requires androgen receptor function. Proc. Natl. Acad. Sci. USA *101*, 1673–1678.

Shang, Y., and Brown, M. (2002). Molecular determinants for the tissue specificity of SERMs. Science *295*, 2465–2468.

Shiina, H., Matsumoto, T., Sato, T., Igarashi, K., Miyamoto, J., Takemasa, S., Sakari, M., Takada, I., Nakamura, T., Metzger, D., et al. (2006). Premature ovarian failure in androgen receptor-deficient mice. Proc. Natl. Acad. Sci. USA *103*, 224–229.

Simpson, E.R., and Davis, S.R. (2001). Minireview: aromatase and the regulation of estrogen biosynthesis–some new perspectives. Endocrinology *142*, 4589–4594.

Sims, N.A., Clement-Lacroix, P., Minet, D., Fraslon-Vanhulle, C., Gaillard-Kelly, M., Resche-Rigon, M., and Baron, R. (2003). A functional androgen receptor is not sufficient to allow estradiol to protect bone after gonadectomy in estradiol receptor-deficient mice. J. Clin. Invest. *111*, 1319–1327.

Smith, E.P., Boyd, J., Frank, G.R., Takahashi, H., Cohen, R.M., Specker, B., Williams, T.C., Lubahn, D.B., and Korach, K.S. (1994). Estrogen resistance caused by a mutation in the estrogen-receptor gene in a man. N. Engl. J. Med. *331*, 1056–1061.

Sun, L., Peng, Y., Sharrow, A.C., Iqbal, J., Zhang, Z., Papachristou, D.J., Zaidi, S., Zhu, L.L., Yaroslavskiy, B.B., Zhou, H., et al. (2006). FSH directly regulates bone mass. Cell *125*, 247–260.

Suzawa, M., Takada, I., Yanagisawa, J., Ohtake, F., Ogawa, S., Yamauchi, T., Kadowaki, T., Takeuchi, Y., Shibuya, H., Gotoh, Y., et al. (2003). Cytokines suppress adipogenesis and PPAR-gamma function through the TAK1/TAB1/NIK cascade. Nat. Cell Biol. *5*, 224–230.

Syed, F., and Khosla, S. (2005). Mechanisms of sex steroid effects on bone. Biochem. Biophys. Res. Commun. *328*, 688–696.

Takeda, S., Elefteriou, F., Levasseur, R., Liu, X., Zhao, L., Parker, K.L., Armstrong, D., Ducy, P., and Karsenty, G. (2002). Leptin regulates bone formation via the sympathetic nervous system. Cell *111*, 305–317.

Takezawa, S., Yokoyama, A., Okada, M., Fujiki, R., Iriyama, A., Yanagi, Y., Ito, H., Takada, I., Kishimoto, M., Miyajima, A., et al. (2007). A cell cycle-dependent co-repressor mediates photoreceptor cell-specific nuclear receptor function. EMBO J. *26*, 764–774.

Teitelbaum, S.L. (2006). Osteoclasts; culprits in inflammatory osteolysis. Arthritis Res. Ther. *8*, 201.

Teitelbaum, S.L. (2007). Osteoclasts: what do they do and how do they do it? Am. J. Pathol. *170*, 427–435.

Teitelbaum, S.L., and Ross, F.P. (2003). Genetic regulation of osteoclast development and function. Nat. Rev. Genet. *4*, 638–649.

Tolar, J., Teitelbaum, S.L., and Orchard, P.J. (2004). Osteopetrosis. N. Engl. J. Med. *351*, 2839–2849.

Windahl, S.H., Andersson, G., and Gustafsson, J.A. (2002). Elucidation of estrogen receptor function in bone with the use of mouse models. Trends Endocrinol. Metab. *13*, 195–200.

Yoshizawa, T., Handa, Y., Uematsu, Y., Takeda, S., Sekine, K., Yoshihara, Y., Kawakami, T., Arioka, K., Sato, H., Uchiyama, Y., et al. (1997). Mice lacking the vitamin D receptor exhibit impaired bone formation, uterine hypoplasia and growth retardation after weaning. Nat. Genet. *16*, 391–396.

Zaman, G., Jessop, H.L., Muzylak, M., De Souza, R.L., Pitsillides, A.A., Price, J.S., and Lanyon, L.L. (2006). Osteocytes use estrogen receptor alpha to respond to strain but their ERalpha content is regulated by estrogen. J. Bone Miner. Res. *21*, 1297–1306.

Accession Numbers

Microarray can be seen in Gene Expression Omnibus under accession number GSE7798.

nature cell biology

DEAD-box RNA helicase subunits of the Drosha complex are required for processing of rRNA and a subset of microRNAs

Toru Fukuda[1,6], Kaoru Yamagata[1,2,6], Sally Fujiyama[1,2,6], Takahiro Matsumoto[1,2], Iori Koshida[1], Kimihiro Yoshimura[1], Masatomo Mihara[1], Masanori Naitou[3], Hideki Endoh[3], Takashi Nakamura[1,2], Chihiro Akimoto[1], Yoko Yamamoto[1], Takenobu Katagiri[4], Charles Foulds[5], Shinichiro Takezawa[1], Hirochika Kitagawa[1], Ken-ichi Takeyama[1], Bert W. O'Malley[5] and Shigeaki Kato[1,2,7]

MicroRNAs (miRNAs) control cell proliferation, differentiation and fate through modulation of gene expression by partially base-pairing with target mRNA sequences[1–6]. Drosha is an RNase III enzyme that is the catalytic subunit of a large complex that cleaves pri-miRNAs with distinct structures into pre-miRNAs[7]. Here, we show that both the p68 and p72 DEAD-box RNA helicase subunits[8–10] in the mouse Drosha complex are indispensable for survival in mice, and both are required for primary miRNA and rRNA processing. Gene disruption of either *p68* or *p72* in mice resulted in early lethality, and in both *p68*$^{-/-}$ and *p72*$^{-/-}$ embryos, expression levels of a set of, but not all, miRNAs and 5.8S rRNA were significantly lowered. In *p72*$^{-/-}$ MEF cells, expression of p72, but not a mutant lacking ATPase activity, restored the impaired expression of miRNAs and 5.8S rRNA. Furthermore, we purified the large complex of mouse Drosha and showed it could generate pre-miRNA and 5.8S rRNA *in vitro*. Thus, we suggest that DEAD-box RNA helicase subunits are required for recognition of a subset of primary miRNAs in mDrosha-mediated processing.

DEAD-box RNA helicases unwind RNA and alter RNA structures through ATP binding and hydrolysis[8–10]. Two members of the family, p68 and p72, have been implicated in many biological events[11–17]. p68 and p72 function may facilitate processing of RNA, particularly miRNA, as generation of miRNAs from primary miRNAs (pri-miRNA) with diverse structures seems to require many RNA-associated factors for RNase III-mediated processing. miRNAs control cell proliferation, differentiation and fate through modulation of gene expression by partially base-pairing with target mRNA sequences[1–6,18]. Mammalian miRNA genes are initially transcribed as mono- or polycistronic precursor pri-miRNAs. Pri-mRNAs are processed into 60–70 nucleotide hairpins with 3′-overhangs by nuclear RNase III endonuclease Drosha to form pre-miRNAs[1,4,7]. Pre-miRNAs translocate into the cytosol and are then processed by Dicer, another RNase III-related enzyme, to form mature 17–24 nucleotide miRNAs[1–7]. Recently, the functional unit of human Drosha (hDrosha) was biochemically identified[7], and it was revealed that hDrosha forms two types of complexes. The smaller di-subunit complex (Drosha plus DGCR8), Microprocessor, mediates genesis of 5.8S rRNA and pre-miRNA from pri-miRNA[7]. The other larger hDrosha complex comprises multiple classes of RNA associated proteins including DEAH-box RNA helicases, heterogeneous nuclear ribonucleoproteins (hnRNP) and several proteins with RNA binding or RRM motifs. p68–p72 ATP-dependent DEAD-box RNA helicases are also components of the larger hDrosha complex[7]. The precise role of the large complex components, particularly the RNA-associated proteins, in processing of pri-miRNA and rRNA remains to be investigated.

The genes for the *p68* and *p72* DEAD-box RNA helicases were disrupted in mice using a conventional method (see Supplementary Information, Fig. S1). The human homologues (DDX5 for p68, refs 8, 9; and DDX17 for p72, ref. 10) are the subunits for the large hDrosha complex[7]. Although no clear phenotypic abnormalities were detected in *p68*$^{+/-}$ and *p72*$^{+/-}$ mice (data not shown), embryonic lethality was observed in *p68*$^{-/-}$ embryos at ~E11.5, and neonatal death occured in *p72*$^{-/-}$ pups (Fig. 1a) at postnatal day 2 (P2) with smaller body size (see Supplementary Information, Fig. S1f). Double disruption of *p68* and *p72* seemed to lead to earlier lethality than *p68* inactivation alone in embryos (Fig. 1a). Ubiquitous expression of p68 and p72 was observed in developing embryos (Fig. 1b). Irrespective of early lethality of the

[1]Institute of Molecular and Cellular Biosciences, University of Tokyo, Yayoi 1-1-1, Bunkyo-ku, Tokyo 113-0032, Japan. [2]ERATO, Japan Science and Technology, Honcho 4-1-8, Kawaguchi, Saitama 332-0012, Japan. [3]Applied Genomics, Molecular Medicine Labs., Drug Discovery Research, Astellas Pharma Inc., 21,Miyukigaoka, Tsukuba-shi, Ibaraki 305-8585, Japan. [4]Research Center for Genomic Medicine, Saitama Medical School, Yamane 1397-1, Hidakashi, Saitama, 350-1242, Japan. [5]Department of Molecular and Cellular Biology, Baylor College of Medicine, One Baylor Plaza, Houston, TX 77030, USA.
[6]These authors contributed equally to this work.
[7]Correspondence should be addressed to S.K. (e-mail: uskato@mail.ecc.u-tokyo.ac.jp)

Received 26 February 2007; accepted 27 March 2007; published online 15 April 2007; DOI: 10.1038/ncb1577

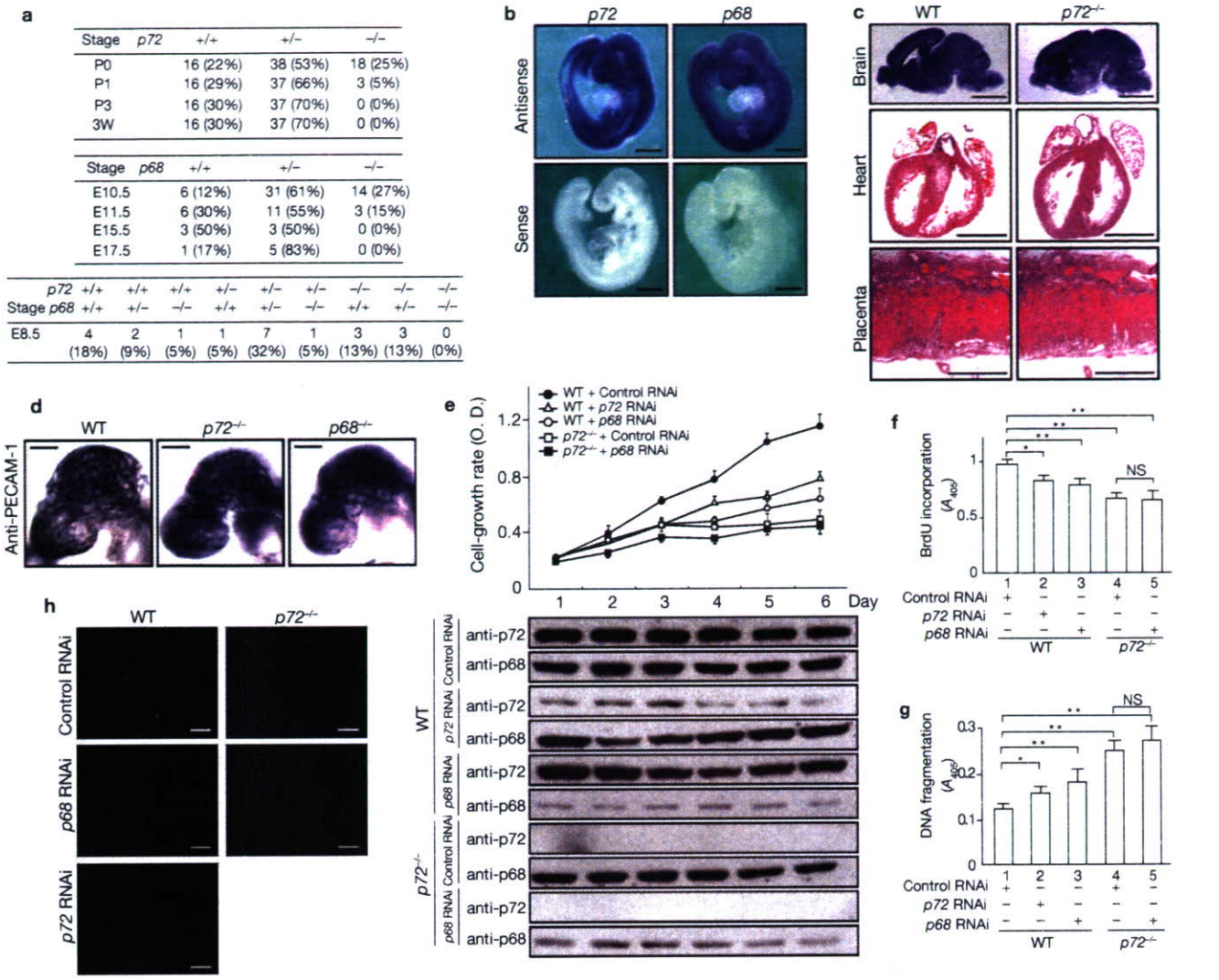

Figure 1 Embryonic and neonatal lethality of *p68* and *p72* knockout mice. (**a**) Genotype of F2 offspring from heterozygous and double (*p68* and *p72*) heterozygous matings. (**b**) Whole-mount *in situ* hybridization of *p72* and *p68* mRNA in wild-type (WT) embryos (E9.5). (**c**) Histological analysis of wild-type and $p72^{-/-}$ embryos (E18.5). Sections were stained with thionine (brain), and hematoxylin and eosin (heart and placenta). (**d**) Immunostaining with anti-PECAM-1 antibody. Wild-type, $p72^{-/-}$ and $p68^{-/-}$ mouse embryos were stage-matched to controls by somite count. (**e**) Analysis of cell-growth rate by modified MTT assay. Results are expressed as the mean ± s.d. of six independent experiments. Protein levels of p72 and p68 for 6 days were confirmed by western blotting. Uncropped images of the blots are shown in the Supplementary Information, Fig. S5a. (**f**) BrdU incorporation of wild-type and $p72^{-/-}$ MEFs with depletion of *p72* and *p68*. Results are expressed as the mean ± s.d. of six independent experiments. Significant differences when compared with the data for wild-type or $p72^{-/-}$ MEFs with control RNAi are shown (single asterisk indicate $P<0.05$; double asterisks indicate $P<0.01$ with one-way ANOVA). NS, not significant. (**g**) Apoptosis was measured by quantification of DNA fragmentation. Results are expressed as the mean ± s.d. of six independent experiments. Significant differences when compared with the data for wild-type or $p72^{-/-}$ MEFs with control RNAi are shown (single asterisk indicates $P<0.05$; double asterisks indicate $P<0.01$with one-way ANOVA). (**h**) TUNEL staining of wild-type and $p72^{-/-}$ MEFs with the indicated RNAi. The scale bars represent 250 μm in **b**, 1 mm in **c**, 150 μm in **d** and 200 μm in **h**.

homozygous mutants, no specific degeneration in organogenesis was detectable (Fig. 1c). Staining with a PECAM-1 antibody showed *p68–p72* homozygous-mutant embryos suffered malformation of blood vessels (Fig. 1d), as previously observed in mice with genetically reduced Dicer activity[19]. Assuming the putative role of the hDrosha complex is in processing of rRNA and miRNAs involved in cellular proliferation, differentiation and cell fate, we first examined cell-growth rates in mouse embryonic fibroblasts (MEFs) from $p72^{-/-}$ embryos. A severe reduction in cell-growth rate because of p72 deficiency was observed (Fig. 1e), and was confirmed by significantly impaired DNA synthesis in $p72^{-/-}$ MEFs, as measured by BrdU incorporation (Fig. 1f). In addition, a clear increase in cell death, as measured by TUNEL staining, was observed in $p72^{-/-}$ MEFs, which was further promoted by *p68* RNA interference (RNAi; Fig. 1g, h).

It has been suggested that the large hDrosha complex containing p68–p72 may, at least in part, excise pri-miRNAs into pre-miRNAs, and cleave preribosomal RNA[7,19–21]. As expression of mature miRNAs was shown to be reduced in human cultured cells deficient in Drosha[20], a global survey of miRNA microarray data was performed to assess expression of miRNAs (www.sanger.ac.uk/Software/Rfam/mirna/index.shtml) in $p72^{-/-}$ embryos at E18.5 (ref. 22). A particular set (94) of pri-miRNAs, but not all surveyed (266), were affected by p72 deficiency (more than 1.5

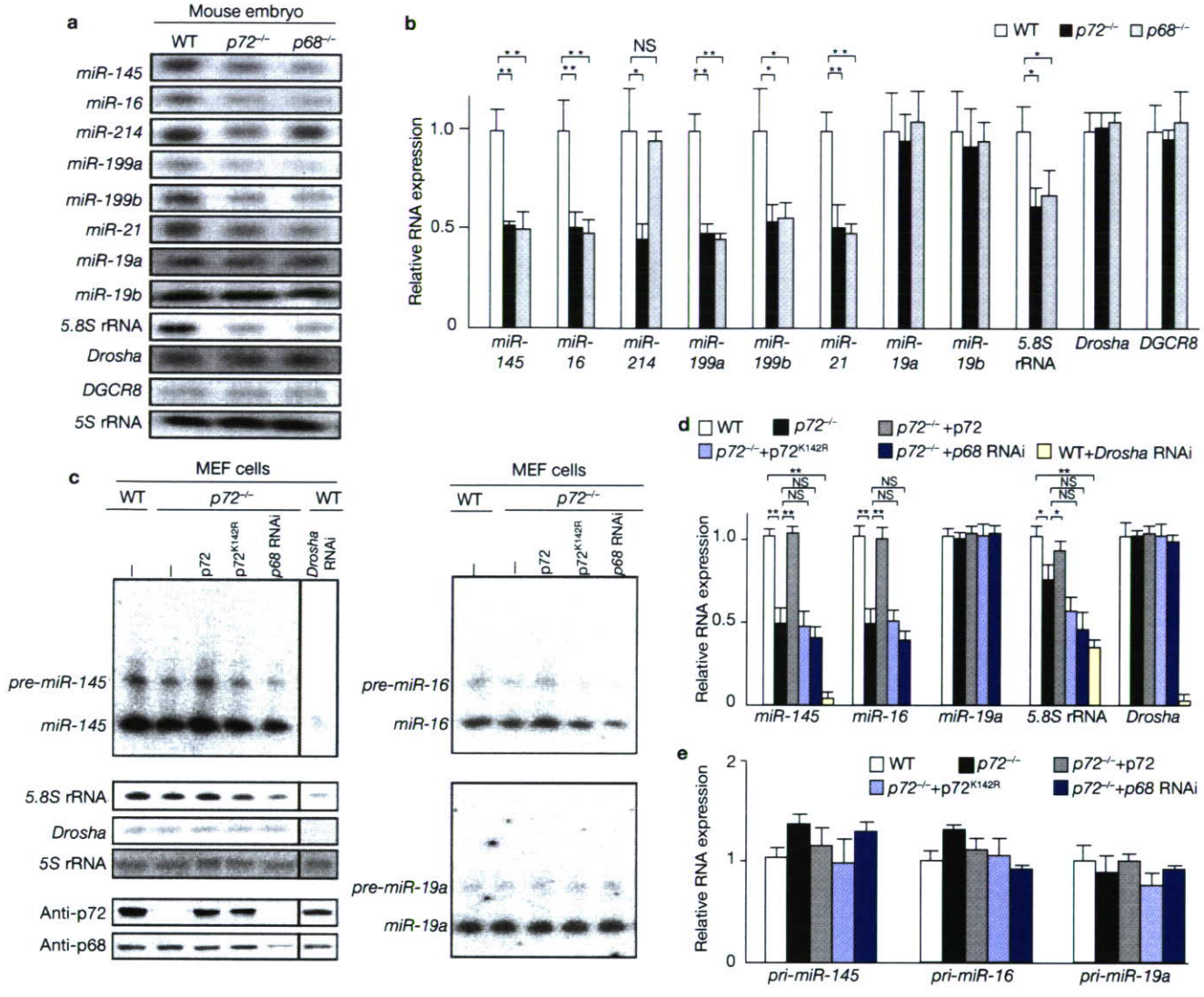

Figure 2 The role of RNA helicases p72 and p68 in miRNA or rRNA processing. (**a**) Northern blot analysis of miRNAs and 5.8S rRNA. Total RNA from wild-type, *p72*$^{-/-}$ and *p68*$^{-/-}$ mouse embryos (E9.5) were purified, and each RNAs were detected by specifc probes as miRNAs, *5.8S* rRNA, *Drosha*, *DGCR8* or *5S* rRNA. (**b**) Results from **a** are expressed as the mean ± s.d. of four independent experiments. Significant differences when compared with the data for wild-type and *p72*$^{-/-}$ or *p68*$^{-/-}$ are shown (single asterisks indicate $P<0.05$; double asterisks indicate $P<0.01$ with one-way ANOVA). (**c**) Northern blot analysis of *miRNA-145*, *miRNA-16*, *miRNA-19a*, *5.8S* rRNA, *Drosha* and *5S* rRNA. Total RNA from wild-type or *p72*$^{-/-}$ MEFs transfected with or without the indicated expression vectors were prepared, and each RNA was detected by specific probes as miRNAs, *5.8S* rRNA, *Drosha*, *DGCR8* or *5S* rRNA. The p72 and p68 expression levels in wild-type or *p72*$^{-/-}$ MEFs, with or without the indicated expression vectors, were detected by western blot analysis. Uncropped images of the blots are shown in the Supplementary Information, Fig. S5b. (**d**) Results from **c** are expressed as the mean ± s.d. of four independent experiments. Significant differences when compared with the data for wild-type or *p72*$^{-/-}$ MEFs are shown (single asterisks indicate $P<0.05$, double asterisk indicates $P<0.01$ with one-way ANOVA). (**e**) Quantitative RT–PCR analysis of *pri-miR-145*, *15* and *19a* expression in wild-type or *p72*$^{-/-}$ MEFs with indicated expression vectors. Results are expressed as the mean ± s.d. of six independent experiments.

times lowered; see Supplementary Information, Fig. S2). To search homologous motif in the regulated 94 miRNAs, a DNA clustering program (DIALIGN2.2.1, available at http://bibiserv.techfak.uni-bielefeld.de/dialign/) was used. Clustering analysis of the two data sets, revealed no continuous consensus sequence among the miRNAs examined. Expression of several of the miRNAs was detectable at significant levels by northern blot analysis. Deficiency of either p68 or p72 was found to reduce expression levels of *miR-145*, *miR-16*, *miR-199a*, *miR-199b* and *miR-21* to almost half of those in the wild-type littermate embryos (Fig. 2a, b). Likewise, expression levels of 5.8S rRNA were reduced in both homozygous embryos (Fig. 2a, b). However, unlike the miRNAs described above, the expression levels of *miR-19a*, *miR-19b* (Fig. 2a, b), and *miR-32*, *miR-128*, *miR-141* and *miR-146* (data not shown) seemed unaffected by p68–p72 deficiency, and *miR-214* expression was reduced only in *p72*$^{-/-}$, but not in *p68*$^{-/-}$ (Fig. 2a, b).

To verify the putative function of p68 and p72 in RNA processing in embryos, expression levels of these RNAs were then measured in MEF cells from *p72*$^{-/-}$ and wild-type littermate embryos. As expected, a significant reduction in the expression levels of the examined miRNAs and 5.8S rRNA because of p72 deficiency was detected (Fig. 2c, d). Knockdown of Drosha by RNAi (see Supplementary Information, Fig. S3c) caused a reduction in the miRNA expression level (Fig. 2c), as expected. However,

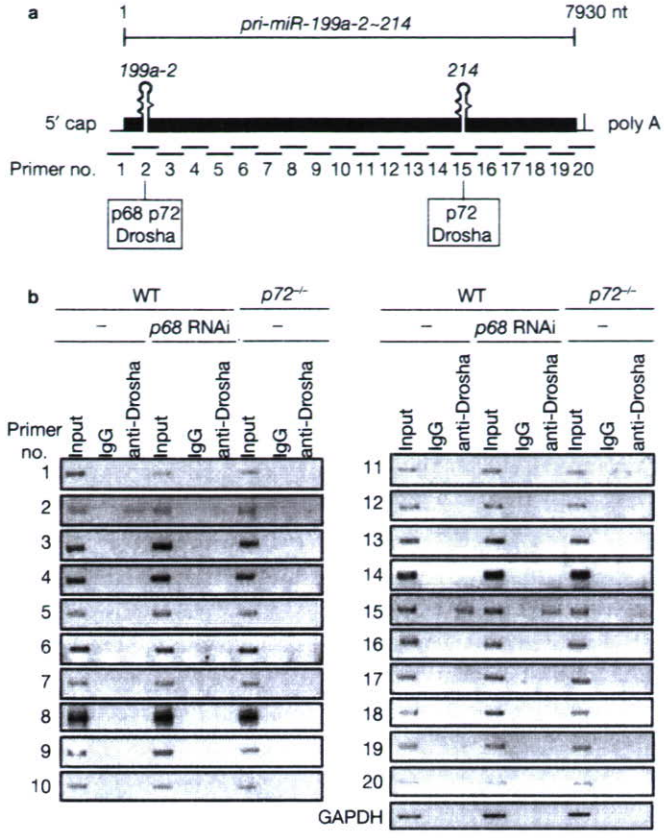

Figure 3 *In vivo* association of the Drosha complex with pri-miRNAs through p68–p72. (**a**) Schematic representation of *pri-miR-199a-2/-214* with the hairpin structure. The numbers (1–20) under the pri-miRNA indicate the amplified region by PCR with specific primer pairs used for RNA–ChIP analysis in **b**. Binding sites for p68–p72 and Drosha in *pri-miR-199a-2/-214* deduced from the RNA–ChIP analysis in **b** are also indicated. (**b**) RNA–ChIP analysis of p68–p72 and Drosha binding sites in *pri-miR-199a-2/-214*. ChIP samples were prepared from wild-type MEFs transfected with *p68* RNAi or not, and from *p72*$^{-/-}$ MEFs. RT–PCR was performed with either total input RNA, RNA precipitated with IgG (negative control) or anti-Drosha antibody.

pri-miRNA-145, *pri-miRNA-16* and *pri-miR-19a* gene expression seemed unaffected by *p72* deficiency plus *p68* RNAi knockdown (Fig. 2e), suggesting that the reduced miRNA levels were not caused by reduced gene expression. Ectopic expression of p72 in *p72*$^{-/-}$ MEFs was sufficient to restore expression levels of the RNAs, whereas such recovery was not induced by expression of a p72 mutant (p72^{K142R}; Fig. 2c, d). p72^{K142R} lacks the putative ATPase activity that is believed essential for RNA helicase activity[10,17]. Knockdown of *p68* and *p72* in the wild-type MEFs clearly lowered expression levels of the miRNAs and 5.8S rRNA, as expected (see Supplementary Information, Fig. S3a), and rRNA processing was significantly affected by *Drosha* RNAi (Fig. 2c). Interestingly, expression levels of *miR-19a* were again unaltered when expression levels of p68–p72 were modulated.

We then addressed the *in vivo* association of pri-miRNAs with p68–p72 in the Drosha complex using an RNA–chromatin immunoprecipiation (ChIP) assay with an mouse Drosha (mDrosha)-specific antibody[23] (Fig. 3b). Using several sets of primers, *in vivo* association of *pri-miR-214* and *pri-mR-16* with Drosha was detected, and the associating regions of pri-miRNAs were mapped (Fig. 3a, b for *pri-miR-214* and see Supplementary Information, Fig. S3b for *pri-miR-16*), although no clearly homologous RNA sequence was present in these regions. Such association was impaired, as expected, in *p72*$^{-/-}$ MEFs and wild-type MEFs with *p68* knocked down by RNAi (Fig. 3b).

To verify the role of the p68–p72 subunits in the mDrosha complex *in vitro*, the association of endogenous p68–p72 with endogenous mDrosha was confirmed by coimmunoprecipitation (Fig. 4a). DGCR8 coimmunoprecipitated with mDrosha as expected. Using a biochemical approach[24,25], the Drosha complex (Fig. 4b) was purified from nuclear extracts of MCT mouse kidney proximal tubule cells stably expressing Flag- and His-tandem tagged mDrosha at a similar expression level to that of endogenous mDrosha (see Supplementary Information, Fig. S2d). The purified mDrosha complex was present in a single complex with a relative molecular mass of over 670,000 when fractionated on a glycerol density gradient (Fig. 4b). Fractionation of total nuclear extracts with western blotting also showed comigration of endogenous Drosha with DGCR8 and p68–p72 at the similar molecular masses with the purified mDrosha complex (Fig. 4c). These findings are consistent with a previous report that the Drosha complex was biochemically isolated as one large complex from S2 insect cells[26]. However, the small complex corresponding to the human Microprocessor complex was undetectable. Even under more stringent conditions (such as at higher salt concentrations), the smaller mDrosha complex was biochemically undetectable in our hands (data not shown). Using mass spectrometric sequencing, p68–p72, several RNPs and mouse DGCR8 were identified (Fig. 4d), and all of the examined subunits were detected by western blotting analysis (Fig. 4b). Two-step column purification of mDrosha complex identified the same subunits (Fig. 4e), supporting previous reports that p68–p72 form a complex[7,27]. As the subunit composition of the purified mDrosha complex accurately reflects the reported composition of the large hDrosha complex components, we presumed that mDrosha forms one large complex similar to the large hDrosha complex.

We then examined whether this purified large complex mediates the processing of miRNA *in vitro*. The purified complex from fraction 7 (Fr. 7) on the glycerol density gradient (see Fig. 4b), as well as the immunoprecipitates of Drosha (Flag–His–mDrosha; Fig. 5a), were able to cleave *miR-16* and *miR-145* pri-miRNAs into pre-miRNAs (Fig. 5b), but not mRNAs (see Supplementary Information, Fig. S4a). Cleavage products of pre-miRNAs were of the expected size (70 nucleotides for *miR-145*, 93 nucleotides for *miR-16*) and 5.8S rRNA (157 nucleotides) was generated from 12S rRNA *in vitro* (Fig. 5b)[21]. However, conversion efficiency of this *in vitro* RNA processing was unexpectedly low, even for longer incubations (Fig. 5c), raising the possibility that a coregulatory subunit for the mDrosha complex may be lost during biochemical purification. Such *in vitro* RNA processing activity of the purified complex (Fr. 7) was significantly attenuated by specific antibodies for p68–p72, as well as mDrosha (Fig. 5d), and by the presence of an ATP analogue (see Supplementary Information, Fig. S4b, c), supporting ATP dependency (Fig. 5e). Furthermore, the complex deficient of either p68 or p72, purified from stable transformants knocked down with RNAi, was impaired in RNA processing (Fig. 5f). This confirms the significance of p68–p72 subunits within the mDrosha complex in RNA processing.

In this study, early lethality of *p68*$^{-/-}$ and *p72*$^{-/-}$ mice clearly establishes the physiological significance of DEAD-box RNA helicases in survival. The physiological impact of p68–p72 on cell differentiation, proliferation and cell fate was also observed in MEFs. Most importantly, the processing of a set of miRNAs and rRNA seemed to

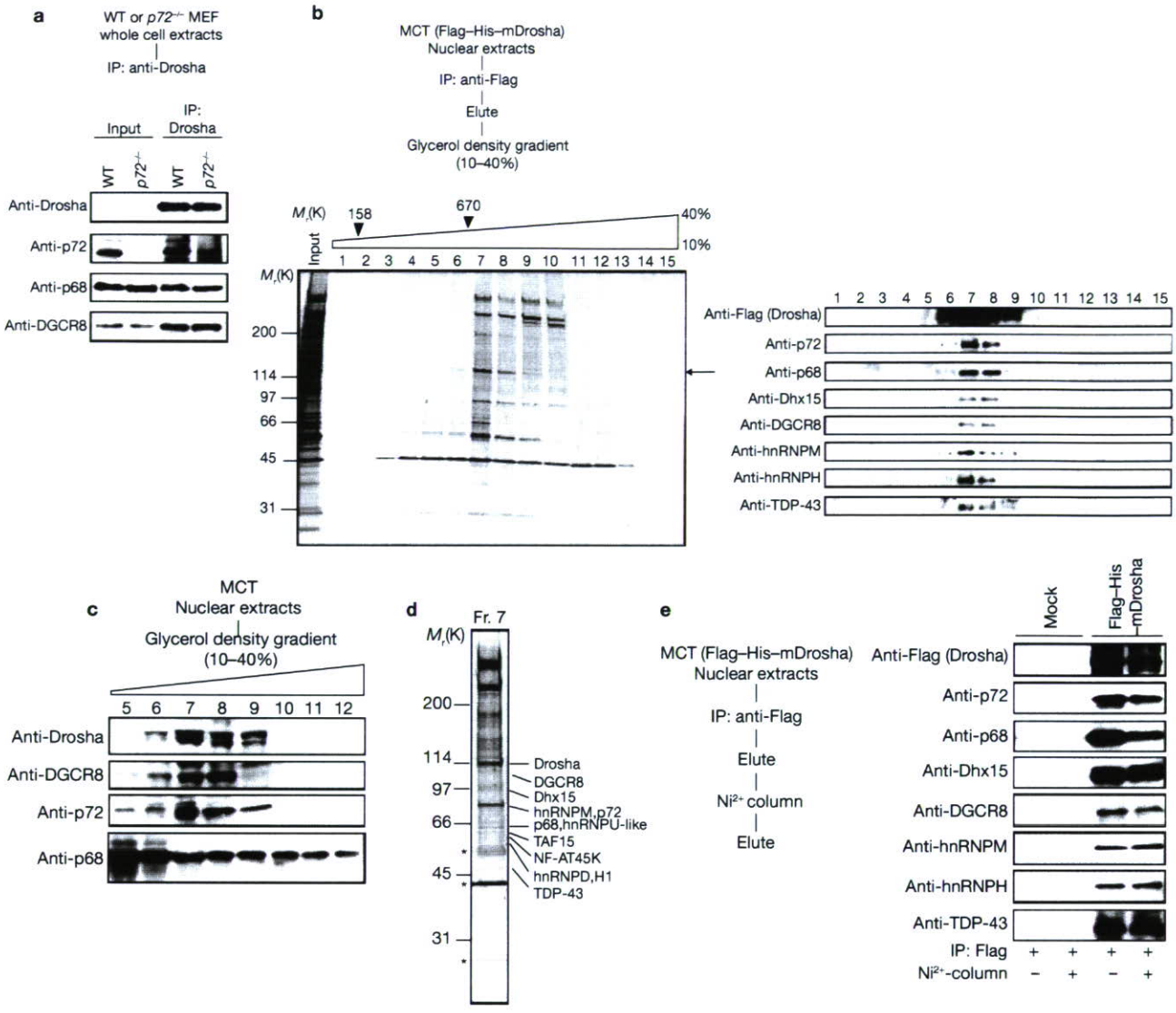

Figure 4 Biochemical isolation of mouse Drosha-containing complex. (**a**) Coimmunoprecipitation of p68–p72 with mDrosha. Whole-cell extracts from MEFs (wild-type and *p72*$^{-/-}$) were prepared for immunoprecipitation (IP) with endogenous mDrosha followed by western blotting (IB). Input, 5% of the cell extracts for immunprecipitiation. Uncropped images of the blots are shown in the Supplementary Information, Fig. S5c. (**b**) Biochemical isolation of mouse Drosha-containing complexes. Silver staining and western blot analysis of glycerol density-gradient fractions are displayed. Molecular masses of marker proteins and fraction numbers are indicated. Fraction 7 was used for mass spectrometric analysis and *in vitro* RNA processing. Input, 5% of the input for glycerol density gradient. The arrow indicates Flag–His–mDrosha. (**c**) Endogenous mDrosha, DGCR8, p72 and p68 cosediment at the same fractions with the Flag–His–mDrosha complex on glycerol density gradients. (**d**) Mass spectrometric identifications of the components in Fr. 7 Flag–His–mDrosha complex in **b**. Asterisks indicate background bands. (**e**) Identification of mDrosha complex components in the mDrosha immunoprecipitant. The Flag–His–mDrosha complex was collected from the nuclear extracts using an anti-Flag antibody column, then repurified by Ni^{2+} affinity chromatography. The complex components were analysed by western blot.

be impaired in both of the homozygous mutants (Fig. 2a, b and see Supplementary Information, Fig. S2). Currently, it remains unclear whether the cellular function of affected miRNAs as a result of *p68–p72* knockout is related to early lethality observed in *p68*$^{-/-}$ and *p72*$^{-/-}$ mice. However, considering the previous report that mouse embryogenesis in the absence of Dicer ceases at an earlier stage (E7.5)[28], normal expression of miRNAs may be essential for survival. Furthermore, the purified mDrosha complex containing p68–p72 was capable of generating a set of processed pre-miRNAs and rRNA through p68 and p72 using an *in vitro* assay (Fig. 5b). Impaired miRNA processing was detected for several, but not all, of the examined miRNA species. Therefore, we speculate that p68–p72 DEAD-box RNA helicases serve as miRNA species-selective subunits in the conversion of pri-miRNA into pre-miRNA by specific recognition of a certain structure of pri-miRNA. This hypothesis is supported by a previous report that the double-stranded RNA-binding protein partner of Drosha (Pasha) is required for insect Drosha-mediated pri-miRNA processing[26]. In this respect, it would be interesting to know whether the cellular functions of the specific miRNAs species processed by p68–p72 correlate with the putative biological functions of p68–p72 (refs 11–17).

Different sets of RNA-associated protein subunits may be required for the processing of other miRNA species[29]. Notably, in the p68–p72 homozygous mutants, the expression levels of several miRNAs were reduced to only half of the wild-type littermates. Therefore, we

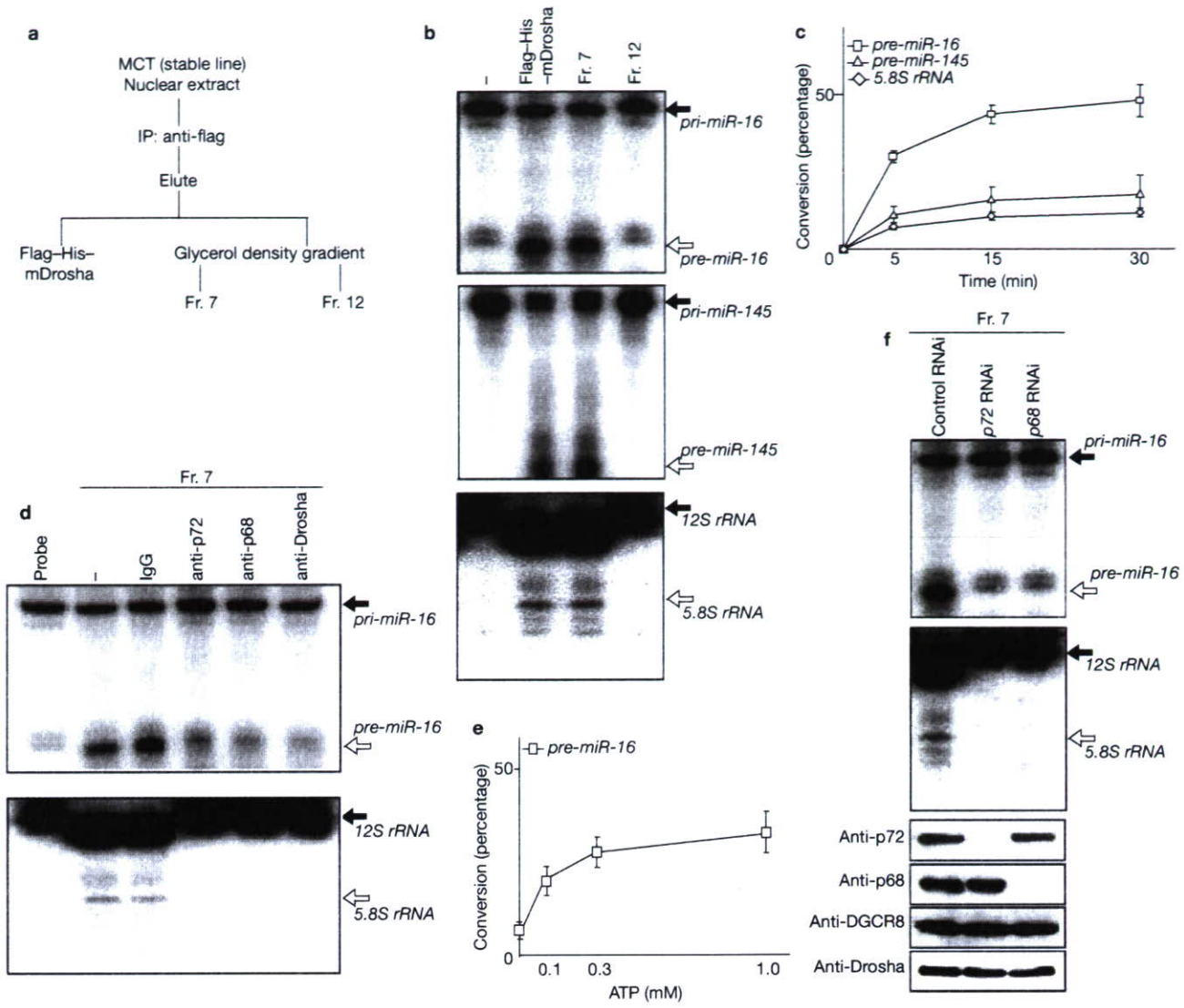

Figure 5 Purified mDrosha complex mediates processing of miRNA and rRNA *in vitro*. (**a**) Schematic representation of the preparation of the samples used in **b**. (**b**) *In vitro* processing analysis of *pri-miR-16*, *pri-miR-145* and *12S* rRNA with Flag–HIS–mDrosha immunocomplexes, fractionated mDrosha complex (Fr. 7), mDrosha-negative fraction (Fr. 12) or negative control (–). Closed arrows and opened arrows indicate the precursor RNA and processed RNA, respectively. (**c**) Time-course conversion rate of *pre-miR-16*, *pre-miR-145* and *5.8S* rRNA (diamond) by purified mDrosha complex (Fr. 7). Results are expressed as the mean ± s.d. of three independent experiments. (**d**) Specific antibodies for p68, p72 and mDrosha attenuated the *pri-miR-16* and *12S* rRNA cleavage by the purified mDrosha complex (Fr. 7). All studies were repeated three times. Probe, input of the substrate *pri-miR-16*; –, Fr. 7 only; IgG, negative control. Closed arrows and opened arrows indicate the precursor RNA and processed RNA, respectively. (**e**) ATP concentration-dependent effect on the *pri-miR-16* cleavage by purified mDrosha complex (Fr. 7). Results are expressed as the mean ± s.d. of three independent experiments. (**f**) *In vitro* processing analysis of *pri-miR-16* and *12S* rRNA with the purified mDrosha complexes prepared from Flag–His–mDrosha stable cells transfected with control RNAi, *p72* RNAi or *p68* RNAi. Western blotting indicates the presence of each complex component. Closed arrows and opened arrows indicate the precursor RNA and processed RNA, respectively. Uncropped images of the blots are shown in the Supplementary Information, Fig. S5d.

speculate that there is possible functional redundancy of p68–p72 with other RNA processing subunits. As it is known that nuclear complexes often form subclasses through association of core components with regulatory subunits[30,31], we cannot exclude the possibility that Drosha–DGCR8 exist as multiple complexes differentially combined with RNA-associated protein subunits in mammals. Furthermore, the subunit composition of the Drosha complex may be developmentally modulated, and thereby cell-type specific.

It remains unclear how the p68–p72 subunits support RNA processing activity of the complex. p68–p72 may function to specifically recognize and stably bind to certain structures of pri-miRNAs and 12S pre-rRNA, and to initiate cleavage at precise RNA sites by Drosha. As the p72 mutant lacking putative ATPase activity did not potentiate RNA processing (Fig. 2c, d), we suggest that ATPase activity of p68–p72 may be required. p68–p72 ATPase activity is dependent on RNA binding[10,32] and is likely to be critical for RNA-unwinding activity[3]. Therefore, we suggest that ATP-dependent p68–p72-mediated structural alteration of specifically associating protein subunits may lead to presentation of RNAs for cleavage by mammalian Drosha. DGCR8 has been reported to be a critical pri-miRNA-associated subunit for Drosha to precisely recognize miRNA stem-loop structures[7,33]. However, other RNA-associated subunits may recognize distinct cognate pri-miRNA tertiary structures by similar or different mechanisms, thus enabling the Drosha complex to process a number of pri-miRNAs. □

METHODS

Antibodies. The following antibodies were used: p68-ab10261 (Abcam, Cambridge, UK); p72 p72N (ref. 17); PECAM-1 MEC13.3 (BD Bioscience, San Jose, CA); Drosha 07017 (Upstate, Billerica, MA); Flag polyclonal (Sigma, St Louis, MO); TARDBP 2E2-D3 (Abnova, Taipei City, Taiwan); hnRNP H N16 (Santa Cruz Biotechnology, Santa Cruz, CA); DHX15 BL972 (Bethyl Laboratories, Montgomery, TX); hnRNP M1-M4 (Zymed, San Francisco, CA); Actin I19 (Santa Cruz). Anti-DGCR8 antibody was generated against a synthetic peptide corresponding to the carboxy-terminal 20 amino-acid sequence (Operon, Huntsville, AL). Appropriate anti-mouse, anti-rabbit and anti-goat secondary antibodies were obtained from Dako (Glostrup, Denmark).

Isolation of MEFs, MEF growth, BrdU incorporation, TUNEL assay and DNA fragmentation. MEFs were isolated from E13.5 embryos and cultured in DMEM with 10% FBS[34]. For MEF growth experiments, cells were seeded in 96-well plates and growth rates were measured by using Cell Counting Kit-8 (Dojindo Laboratories, Kumamoto, Japan). DNA synthesis was detected and measured in cultured cells by BrdU incorporation using 5′-bromo-2′-deoxy-uridine Labeling and Detection Kit III (Roche Applied Science, Basel, Switzerland). Apoptotic cells were assessed by the DNA terminal nick-end translation method (TUNEL assay) using the DeadEnd Fluorometric TUNEL System (Promega, Madison, WI). For apoptotic cell quantitation, DNA fragmentation was measured by using Cell Death Detection ELISA^{PLUS} (Roche Applied Science). These assays were performed following the manufacturer's instructions.

RNAi depletion of *p68*, *p72* and *Drosha*. Small interfering RNA (siRNA) oligonucleotides of *p68*, *p72* and *Drosha* were used for knockdown of endogenous protein expression using siGENOME (Dharmacon, Lafayette, CO). Four kinds of independent siRNA duplexes were mixed. Their sequences are: *p68* siRNA duplex, sense 5′-GAACUGAGUGCAAACCAUAUU-3′ and antisense 5′-PUAUGGUUUGCACUCAGUUCUU-3′: sense 5′-GCUUGUCGCUUGAAGUCUAUU-3′ and antisense 5′-PUAGACUUCAAGCGACAAGCUU-3′: sense 5′-UCAAUUAUGACUACCCUAAUU-3′ and antisense 5′-PUUAGGGUAGUCAUAAUUGAUU-3′:sense5′-GCGCACCGCACAAGAGGUAUU-3′ and antisense 5′-PUACCUCUUGUGCGGUGCGCUU-3′. *p72* siRNA duplex: sense 5′-GUACUUACCUUGUGUUGGAUU-3′ and antisense 5′-PUCCAACACAAGGUAAGUACUU-3′:sense5′-GAAAGAGAUUGGGUACUUAUU-3′ and antisense 5′-PUAAGUACCCAAUCUCUUUCUU-3′; sense 5′-GGAAGACAUUGGCGUAUUUUU-3′ and antisense 5′-PAAAUACGCCAAUGUCUUCCUU-3′:sense5′-GGGCUAGGUUUGUAUAGAUUU-3′ and antisense 5′-PAUCUAUACAAACCUAGCCCUU-3′. *Drosha* siRNA duplex: sense 5′-CGUGGAGGGUGUUAUAGUAUU-3′ and antisense 5′-PUACUAUAACACCCUCCACGUU-3′:sense5′-CAAUACGUGUCAUAGAAUGUU-3′ and antisense 5′-PCAUUCUAUGACACGUAUUGUU-3′: sense 5′-GAACCUACAUCGUGAGCGGUU-3′ and antisense 5′-PCCGCUCACGAUGUAGGUUCUU-3′:sense5′-GGGACUCUCUAGACUGUGAUU-3′and antisense 5′-PUCACAGUCUAGAGAGUCCCUU-3′. MEFs were transfected with each duplex (25 nM) using SuperFect transfection reagent (Qiagen, Hilden, Germany).

Northern blot analysis and quantitative RT–PCR. Total RNA from embryos or MEFs was prepared in TRIzol reagents (Invitrogen, Carlsbad, CA) in accordance with the manufacturer's instructions. Northern blot analysis was carried out as previously described[35]. *Drosha* cDNA and the following oligonucleotides were used as probes: *miR-145*, 5′-AAGGGATTCCTGGGAAAACTGGAC-3′; *miR-16*, 5′-CGCCAATATTTACGTGCTGCTA-3′; *miR-214*, 5′-CTGCCTGTCTGTGCCTGCTGT-3′; *miR-199a*, 5′-AACCAATGTGCAGACTACTGTA-3′; *miR-199b*, 5′-GAACAGGTAGTCTAAACACTGGG-3′; *miR-21*, 5′-TCAACATCAGTCTGATAAGCTA-3′; *miR-19a*, 5′-TCAGTTTTGCATAGATTTGCACA-3′; *miR-19b*, 5′-TCAGTTTTGCATGGATTTGCACA-3′; *5.8S* rRNA, 5′-TCAGACAGGCGTAGCCCCGGGAGGAACCCG-3′; and *5S* rRNA, 5′-CAGGCCCGACCCTGCTTAGCTTCCGAGATCAGACGAGAT-3′(5S rRNA). Real-time quantitative RT–PCR was performed on an ABI Prism 7900HT Sequence Detector (Applied Biosystems, Foster City, CA). The primers used were as follows: *pri-miR-16*, 5′-CCCTTGGAGTAAAGTAGCAGCA-3′ (forward) and 5′-GTCCTTGTATTTTGAGGCAGCA-3′ (reverse); *pri-miR-19*, 5′-ACTGCCCTAAGTGCTCCTTCTG-3′ (forward) and 5′-GAGGGCTGCAAACACAACTATG-3′(reverse); *pri-miR-145*, 5′-ATGCCGAGAGAACTGCTGGT-3′ (forward) and 5′-AAACTGGACCGTGAGGACAA-3′(reverse); *GAPDH*, 5′-AAATGGTGAAGGTCGGTGTG-3′(forward) and 5′-TGAAGGGGTCGTTGATGG-3′ (reverse). Expression levels were normalized for GAPDH expression.

Purification of Flag–His–mDrosha. Flag–His–mDrosha was transfected into MCT mouse kidney proximal tubule cells. Transfected cells were selected with G418 and individual colonies were isolated and analysed for Flag–His–mDrosha expression. To purify the mDrosha complex, nuclear extract was prepared as described previously[24,25] and applied to the anti-Flag M2 affinity resin (Sigma) column. After washes with buffer A (20 mM Tris–HCl at pH 7.9, 0.5 M KCl, 10% glycerol, 1 mM EDTA, 5 mM DTT, 0.5% NP-40, 0.2 mM PMSF), the affinity column was eluted with 400 μg ml^{-1} Flag peptide in buffer A. Eluted complex was analysed by 10–40% glycerol density gradient centrifugation. Fractions from the glycerol density gradient were concentrated by precipitation with trichloroacetic acid and analysed by SDS–PAGE followed by silver staining and western blotting[24,25]. For two-step purification, Flag-eluted complex was applied to HIS–Select nickel affinity gel (Sigma). After washes with 0.8× LEW buffer (40 mM NaH_2PO_4 at pH 8.0, 240 mM NaCl), the complex was eluted with elution buffer (50 mM NaH_2PO_4 at pH 8.0, 300 mM NaCl, 250 mM imidazole). For the large mDrosha complex deficient for p68 or p72, *p68* or *p72* was knocked down by RNAi in the stable transformants before the complex purification.

***In vitro* miRNA or rRNA processing analysis.** *In vitro* transcription was carried out using linearized pcDNA3 vector containing *pri-miR-16* or *12S* rRNA[24]. Briefly, the miRNA probes (*pri-miR-16* or *pri-miR-145*) were amplified from embryo RNA by RT–PCR with 5′-TTCAGGGATCCCATGCTAGCAAGAAGCACTTGGCCA-3′ as forward primer and 5′-AACAAGAATTCTGAAAAGGTGCAGGCCATACTGTGC-3′ as reverse primer or 5′-TTCAGGGATCCAAAAGCTATACAAAGGTCAGAAGAG-3′ as forward primer and 5′-AACAAGAATTCTTCCCAGAGCAGGACGCTGCATCCC-3′as reverse primer, respectively. The *12S* rRNA probes were also prepared with 5′-TCTATGGATCCGTCAGAAAGGGGGGACACGCGCCCAGCCGC-3′as forward primer and 5′-TCTATGAATTCCGACTCTTAGCGGTGGATCACTCGGCTCGTG-3′ as reverse primer. The processing reaction, containing the indicated amounts of Drosha complex (immunoprecipitation products or two-step purification products from MCT cells), 3 μl of solution containing 32 mM $MgCl_2$, 10 mM ATP, 2006mM creatine phosphate, 20 U μl^{-1} RNAase inhibitor (Toyobo, Osaka, Japan) and the α^{32}P-UTP-internal-labelled pri-miRNA and buffer (20 mM Tris–HCl at pH 7.9, 0.1 M KCl, 10% glycerol, 5 mM DTT, 0.2 mM PMSF), were added to a final volume of 30 μl, as previously described[7,20], in the absence or presence of hexokinase (Sigma). The reaction mixture was incubated at 37 °C for 90 min and extracted with phenol:chloroform mixture, then with chloroform and precipitated with 300 mM sodium acetate and ethanol. The precipitated RNA was loaded on 15% denaturing polyacrylamide gels, and then autoradiographed.

RNA–ChIP. RNA–ChIP was performed as previously described[23]. All the buffers used in this study contained 0.5 U μl RNase inhibitor. Nuclei from MEF cells (wild-type, *p68*-knocked down wild-type or *p72*$^{-/-}$) were first isolated from 1% formaldehyde-fixed cells and used for chromatin fragmentation. After immunoprecipiation with anti-Drosha antibody, washing and elution, the precipitated RNA–DNA pellets were resuspended in 70 μl nuclease-free water with 1 μl of 40 U μl^{-1} RNase inhibitor, 5 μl of 1 M Tris–HCl at pH 7.5, 20 μl of 50 mM $MgCl_2$, and 4 μl of 10 U μl DNase I. The mixture was incubated for 30 min at 37 °C and extracted once with phenol:chloroform (5:1). RNA was precipitated with ethanol and dissolved in 30 μl of nuclease-free water. Twenty-nine microliters of the RNA was used for a 60 μl cDNA synthesis reaction. The PCR reactions were performed at 33 cycles, which was within the linear range of the amplification. Of 50 μl of product, 6 μl was loaded onto a 1.5% agarose gel, stained with ethidium bromide, and photographed. The primer sequences used are given in the Supplementary Information.

Microarray data. The microarray data can be be seen in ArrayExpress (accession number, E-MEXP-1052; for further details see Supplementary Information, Methods).